Emission Mössbauer spectroscopy and relaxation measurements in hyperfine levels out of thermal equilibrium: Very-low-temperature experiments on the Kondo alloy $Au^{170}Yb$

P. Bonville, P. Imbert and G. Jéhanno
Centre d'Etudes Nucléaires de Saclay, Service de Physique du Solide et de Résonance Magnétique, Commissariat à l'Energie Atomique, F-91191 Gif-sur-Yvette Cédex, France

F. Gonzalez-Jimenez
Departamento de Fisica, Universidad Central de Venezuela, Caracas, Venezuela

F. Hartmann-Boutron
Laboratoire de Spectrométrie Physique (associé au Centre National de la Recherche Scientifique), Université Scientifique et Médicale de Grenoble, Boîte Postale 68, F-38042 Saint Martin d'Hères Cédex, France
(Received 21 February 1984)

Mössbauer emission spectra of the $^{170}Yb^{3+}$ ion were recorded at very low temperatures ($0.09 \leq T \leq 4.2$ K) in $Au^{170}Tm$ sources and were interpreted by means of a relaxation line-shape theory which takes into account the existence of populations out of thermal equilibrium in the hyperfine levels. The relaxation measurements gave confirmation of the Kondo behavior of Yb^{3+} in gold, and the fitted values of $1/(T_1T)$ are in better agreement with an Abrikosov-type variation in $[\ln(T/T_K)]^{-2}$ (with $T_K \sim 10^{-6}$ K) than with a linear dependence in $\ln T$.

I. INTRODUCTION

In recent years the study of the dynamical behavior of localized moments in solids has been performed by means of a variety of spectroscopic techniques: EPR, Mössbauer spectroscopy (MS), NMR, and neutron inelastic scattering (NIS). The methods used in the measurements may be classified within two categories: methods in which a thorough energy analysis of the spectrum is performed and the paramagnetic relaxation rate is extracted from the line shape (EPR, MS, and NIS); and methods in which a perturbation of the thermal-equilibrium populations of the energy levels of the system is used (quick saturation of a transition in EPR, spin echoes in NMR) and the relaxation time is measured by observation of the recovery of these populations toward Boltzmann equilibrium.

In EPR, NIS, and MS local-moment—relaxation studies in dilute alloys, the preferred method is usually the analysis in energy of the impurity spectrum, whereas the "population method" is used in NMR for the measurement of nuclear relaxation times induced by fluctuations of the local moment.

In previous works we used the deformation of the Mössbauer emission spectrum of the ^{170}Yb isotope to measure the paramagnetic relaxation rate of ytterbium impurities in gold between 0.6 and 26 K.[1-3] The measurements provided the first evidence of a logarithmic dependence, due to the Kondo effect, of the thermal variation of a local-moment relaxation rate induced by conduction electrons.[1(b),1(c)] In addition, the Kondo behavior of the dilute alloy AuYb was independently observed by means of resistivity measurements.[4] Later, the presence of logarithmic anomalies in the relaxation frequencies of impurities was also observed by using other spectroscopic techniques in various Kondo systems: CuFe by NIS (Ref. 5) and by NMR (Refs. 6 and 7), CuMn by NMR (Ref. 8), and, recently, AuYb by EPR (Ref. 9).

In a subsequent work[10-12] we showed that measuring the populations of the hyperfine levels out of thermal equilibrium in Mössbauer sources could be used to extend paramagnetic relaxation measurements down to very low temperatures.

In this work we apply the method to the dilute alloy $Au^{170}Yb$, which we studied in a ^{3}He-^{4}He dilution refrigerator down to temperatures below the hyperfine separation $\Delta/k_B \simeq 0.11$ K.

Section II summarizes the formalism required for the interpretation of the low-temperature Mössbauer emission spectra. In order to analyze the spectra recorded between 0.09 and 4.2 K in a continuous way, we developed a new relaxation line-shape calculation, which accounts for the presence of hyperfine populations out of thermal equilibrium and whose validity holds whatever the temperature compared to Δ/k_B. We also calculated a variant line shape with the help of the secular approximation, which enables a more direct interpretation of the relative line intensities and dynamical broadenings to be made near the slow-relaxation regime. The theoretical problems related to the computation of the Mössbauer emission line shape at low temperature in the absence or in the presence of the Kondo effect are presented more thoroughly in Appendixes A—C. In Sec. III we deal with sample preparation and the experimental setup. The experimental results are described and analyzed in Sec. IV. The Mössbauer relaxa-

tion data are interpreted in terms of the Kondo effect and are compared with the recent EPR data of Ref. 9. Finally, in Sec. V we discuss the nature of the interaction between $4f$ and conduction electrons and compare different expressions for the Kondo anomaly of the thermal dependence of the relaxation rate.

II. EMISSION LINE-SHAPE FORMALISM: SUMMARY AND NEW DEVELOPMENTS

A. Main features of Mössbauer spectroscopy in the dilute alloy $Au^{170}Yb$

In order to reduce effects due to the proximity between impurities, low impurity-concentration levels are needed. This, in turn, imposes the recourse to emission experiments rather than absorption experiments. Thus we used very dilute AuTm alloys to study the source $Au(^{170}Tm \rightarrow ^{170}Yb)$ (cf. Sec. III).

The electronic ground state of the $^{170}Yb^{3+}$ ion in the cubic crystalline field of gold is the Kramers doublet Γ_7, and the separation from the excited Γ_6 and Γ_8 states is about 80—90 K.[13] When only the ground Γ_7 level is populated, the hyperfine (hf) Hamiltonian is

$$\mathscr{H}_{\rm hf}=A\vec{I}\cdot\vec{S}\,, \tag{1}$$

where $\vec{S}$ is the effective electronic spin of $\Gamma_7(S=\frac{1}{2})$ and $\vec{I}$ is the nuclear spin of the excited 84.3-keV state of $^{170}Yb(I=2)$, the nuclear spin being 0 in the ground state.

The isotropic hyperfine constant A is (897 ± 5) MHz or (13.20 ± 0.07) mm s^{-1} (cf. Sec. IV). The eigenstates of the Hamiltonian $\mathscr{H}_{\rm hf}$ are two hyperfine multiplets corresponding to the values $F_1=\frac{3}{2}$ and $F_2=\frac{5}{2}$ of the total angular momentum $\vec{F}=\vec{I}+\vec{S}$. These multiplets have degeneracies $2F_1+1=4$ and $2F_2+1=6$, and energies $E_1=-\frac{3}{2}A$ and $E_2=A$. Thus the hyperfine separation is $\Delta=\frac{5}{2}A$, i.e., 2243 MHz, or 33.0 mm s^{-1}, or 0.108 K (Fig. 1).

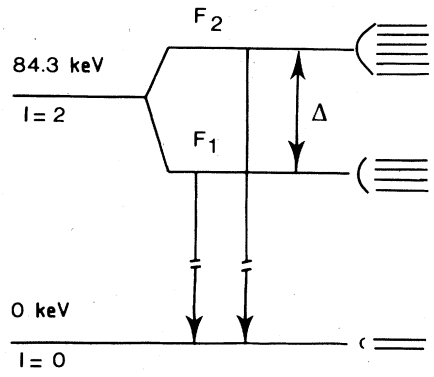

FIG. 1. Hyperfine-level scheme in the Γ_7 state of the $^{170}Yb^{3+}$ ion in a cubic site. The degeneracies of the electronuclear levels are indicated on the right-hand side.

The ^{170}Yb Mössbauer emission spectrum observed from the $Au^{170}Tm$ source in zero external magnetic field depends on the paramagnetic relaxation rate $1/T_1$ between the two states of the electronic doublet Γ_7. In the slow-relaxation regime, i.e., when $1/T_1 \ll \Delta/\hbar$, the spectrum is made of two lines separated by the energy Δ. In the fast-relaxation regime ($1/T_1 \gg \Delta/\hbar$), only one line remains, located at the center of mass of the two above-mentioned slow-relaxation lines. In our previous works[1–3] the intermediate-relaxation spectra ($1/T_1 \sim \Delta/\hbar$) allowed us to measure the relaxation rate $1/T_1$ between 0.6 and 26 K using the method of line-shape analysis in the high-temperature approximation ($k_BT \gg \Delta$). The relaxation frequency band $1/(2\pi T_1)$ so explored ranged from 120 to 9160 MHz, i.e., from about $\frac{1}{18}\Delta/\hbar$ to $4\Delta/\hbar$.

Below about $T=0.5$ K, one cannot maintain the high-temperature assumption. On the contrary, $k_BT \sim \Delta$, and the "spherical relaxation" approximation[2] no longer holds in the relaxation line-shape calculation: one must consider separately spectral densities related to hyperfine "inter-multiplet" and "intramultiplet" transitions. Indeed, the exchange Hamiltonian responsible for relaxation,

$$\mathscr{H}_R=-2\alpha J_{sf}\vec{s}\cdot\vec{S} \tag{2}$$

[$\vec{s}$ being the conduction-electron spin, J_{sf} the exchange constant between $4f$ electrons and conduction electrons, and $\alpha=g(\Gamma_7)(g_J-1)/g_J$, with $g(\Gamma_7)=\frac{24}{7}$ and $g_J=\frac{8}{7}$ for Yb^{3+}], has nonvanishing matrix elements both within a multiplet and between multiplets. Intermultiplet relaxation, due to the inelastic diffusion of conduction electrons on the impurity, involves the spectral densities $J(\pm\Delta)$ at the energy $\pm\Delta$, whereas intramultiplet relaxation involves the spectral density $J(0)$ corresponding to elastic diffusion. In the absence of any Kondo effect, these spectral densities are given by[11,14]

$$\begin{aligned} J(0)&=C_KT\,,\\ J(-\Delta)&=C_K\frac{\Delta}{k_B}\left[\exp\left[\frac{\Delta}{k_BT}\right]-1\right]^{-1}\,,\\ J(\Delta)&=J(-\Delta)\exp\left[\frac{\Delta}{k_BT}\right]\,, \end{aligned} \tag{3}$$

where C_K is the Korringa constant,

$$C_K=\frac{4\pi k_B}{\hbar}[\alpha J_{sf}n(E_F)]^2\,, \tag{4}$$

with $n(E_F)$ the metal density of states at the Fermi level per spin direction.

Furthermore, below $T=0.5$ K, the relaxation rate $1/T_1$ of the Γ_7 doublet of Yb^{3+} in gold becomes much smaller than $\Delta/\hbar=1.41\times10^{10}$ s^{-1} and becomes comparable with the inverse nuclear lifetime $\Gamma=1/\tau_n=0.431\times10^9$ s^{-1} ($\hbar\Gamma=1.01$ mm s^{-1}, or 68.6 MHz, is the natural linewidth of the Mössbauer transition). In this quasi-slow-relaxation regime and at such low temperatures, the hyperfine populations are observed out of thermal equilibrium in emission Mössbauer spectra.

A comprehensive description of the theoretical properties of the electronuclear system in this temperature range (relaxation line shape, density matrix, Kondo behavior) is given in Appendixes A–C. Below, we outline the main features concerning the hyperfine populations and the relaxation line-shape formulas needed for the interpretation of our experimental data.

B. Time evolution of the hyperfine populations

Let $P_1(t)$ and $P_2(t)$ be the respective populations at time t of the F_1 and F_2 hyperfine multiplets, choosing the decay time of the radioactive parent as $t=0$.

As the $^{170}Tm^{3+}$ parent ion in the gold host lattice has a diamagnetic and well-isolated ground state without any hyperfine interaction, the ten hyperfine states of the Yb^{3+} daughter ion receive equal initial populations at time $t=0$. Assuming that each of these populations is normalized to unity, the initial populations P_1^0 and P_2^0 in the F_1 and F_2 multiplets are equal to the respective degeneracies

$$P_1^0=4 \text{ and } P_2^0=6 . \tag{5}$$

As shown in Appendix B, the density matrix of the tenfold hyperfine multiplicity of the excited nuclear state of ^{170}Yb in the source $Au\,^{170}Tm$ remains diagonal during its evolution under the action of the relaxation forces. Evolution of the populations $P_1(t)$ and $P_2(t)$ takes place from the initial values P_1^0 and P_2^0 toward the Boltzmann values,

$$P_1^B=\frac{20}{2+3e^{-\Delta/k_BT}} \text{ and } P_2^B=\frac{30e^{-\Delta/k_BT}}{2+3e^{-\Delta/k_BT}} , \tag{6}$$

but this process is stopped by the decay of the excited nuclear state.

It can be shown[11] that the time evolution of $P_1(t)$ and $P_2(t)$ involves only two intermultiplet transition probabilities,

$$U=\mathscr{P}(F_2\rightarrow F_1) \text{ and } V=\mathscr{P}(F_1\rightarrow F_2) ,$$

obeying the detailed balance rule

$$V/U=\tfrac{3}{2}\exp(-\Delta/k_BT)=P_2^B/P_1^B , \tag{7}$$

and the evolution equations of $P_1(t)$ and $P_2(t)$ are simply

$$\frac{dP_1(t)}{dt}=UP_2(t)-VP_1(t), \quad \frac{dP_2(t)}{dt}=VP_1(t)-UP_2(t) . \tag{8}$$

The actual populations observed by Mössbauer emission spectroscopy are

$$[P_1]_{av}=\frac{1}{\tau_n}\int_0^\infty e^{-t/\tau_n}P_1(t)dt ,$$
$$[P_2]_{av}=\frac{1}{\tau_n}\int_0^\infty e^{-t/\tau_n}P_2(t)dt , \tag{9}$$

that is, after integrating (8) and (9),

$$[P_1]_{av}=\frac{P_1^0+(\tau_n/T_{1hf})P_1^B}{1+\tau_n/T_{1hf}},$$
$$[P_2]_{av}=\frac{P_2^0+(\tau_n/T_{1hf})P_2^B}{1+\tau_n/T_{1hf}} , \tag{10}$$

where $1/T_{1hf}$ is the hyperfine relaxation rate defined by

$$1/T_{1hf}=U+V . \tag{11}$$

The quantities $[P_1]_{av}$ and $[P_2]_{av}$ represent the integrated intensities of the two lines of the quasi-slow-relaxation emission spectrum of $Au\,^{170}Yb$. Under good experimental conditions, direct measurement of these intensities, when $k_BT\sim\Delta$ and $T_{1hf}\sim\tau_n$, allows the determination of $1/T_{1hf}$ with the help of the following equations, derived from relations (10):

$$\frac{1}{T_{1hf}}=\frac{1}{\tau_n}\frac{P_1^0-[P_1]_{av}}{[P_1]_{av}-P_1^B}=\frac{1}{\tau_n}\frac{P_2^0-[P_2]_{av}}{[P_2]_{av}-P_2^B} . \tag{12}$$

This is a "second window" for relaxation-rate measurements centered on the value $\Gamma=1/\tau_n$.[11] A similar method was successfully applied in the $ZnS^{57}Fe^{2+}$ system,[15] where it has been possible to measure phonon-induced relaxation frequencies between electronic levels of the Fe^{2+} ion, from the populations of these levels observed out of thermal equilibrium in Mössbauer emission spectrometry.

The intermultiplet transition probabilities U and V are simply related to the spectral densities $J(\pm\Delta)$ given in relations (3) and they are[11]

$$U=\mathscr{P}(F_2\rightarrow F_1)=\tfrac{4}{10}J(\Delta)=\tfrac{4}{10}C_K\frac{\Delta}{k_B}\frac{e^{\Delta/k_BT}}{e^{\Delta/k_BT}-1} ,$$
$$V=\mathscr{P}(F_1\rightarrow F_2)=\tfrac{6}{10}J(-\Delta)=\tfrac{6}{10}C_K\frac{\Delta}{k_B}\frac{1}{e^{\Delta/k_BT}-1} , \tag{13}$$

which gives

$$\frac{1}{T_{1hf}}=\tfrac{4}{10}J(\Delta)+\tfrac{6}{10}J(-\Delta) , \tag{14}$$

or

$$\frac{1}{T_{1hf}}=\left[(\tfrac{6}{10}+\tfrac{4}{10}e^{\Delta/k_BT})\frac{\Delta}{k_BT}\frac{1}{e^{\Delta/k_BT}-1}\right]C_KT . \tag{15}$$

A numerical calculation shows that the factor in the large parentheses does not depart from the value 1 by more than 3% in the temperature range reached in our experiments ($T\geq 0.09$ K).

Thus we have, to a good approximation,

$$1/T_{1hf}\simeq C_KT , \tag{16}$$

which has the same form as the high-temperature expression ($k_BT\gg\Delta$)

$$1/T_1=C_KT \tag{17}$$

for the electronic relaxation rate $1/T_1$ within the Γ_7 ground-state level.

C. New low-temperature relaxation line shapes

In order to link the measurements of the parameter C_K made in the "first window" [that is, using relation (17) and the high-temperature line shape] with those made in the "second window" [that is, using relations (12) and (15)

or (16) and low-temperature line-intensity measurements], we calculated a general relaxation line shape which applies whatever the temperature compared to Δ/k_B. As the new line shape allows a continuous exploitation of the Au ^{170}Yb emission spectra to be performed in the entire relaxation frequency range, we will no longer refer to first-and second-window-type measurements in the following.

This general line shape, which is derived in Appendix A [relation (A19)], can be written as follows:

$$I(\omega)=\mathrm{Re}\left[\frac{[P_1]_{\mathrm{av}}[p+i(A/\hbar)+(\Delta\Gamma_1+\Delta\Gamma_2)/2]+[P_2]_{\mathrm{av}}[p-3iA/2\hbar+(\Delta\Gamma_1+\Delta\Gamma_2)/2]}{(p+\Delta\Gamma_1/2-3iA/2\hbar)(p+\Delta\Gamma_2/2+iA/\hbar)-\Delta\Gamma_1\Delta\Gamma_2/4}\right], \tag{18}$$

where $p=\Gamma/2-i\omega$, and

$$\Delta\Gamma_1=\tfrac{6}{10}[J(0)+J(-\Delta)]=\tfrac{6}{10}C_K T\left[1+\frac{\Delta}{k_B T}\frac{1}{e^{\Delta/k_B T}-1}\right], \tag{19a}$$

$$\Delta\Gamma_2=\tfrac{4}{10}[J(0)+J(\Delta)]=\tfrac{4}{10}C_K T\left[1+\frac{\Delta}{k_B T}\frac{e^{\Delta/k_B T}}{e^{\Delta/k_B T}-1}\right]. \tag{19b}$$

For $k_B T\gg\Delta$, where the white-noise approximation (WNA) applies, the line shape (18) reduces to the usual high-temperature line shape [Appendix A, relation (A25)].

At low temperature, when the relaxation line broadenings are small compared to the hyperfine separation Δ, one can also compute the line shape within the secular approximation. The "secular line shape" is written[16]

$$I(\omega)=\mathrm{Re}\left[\frac{[P_1]_{\mathrm{av}}}{\frac{1}{2}(\Gamma+\Delta\Gamma_1)-i(\omega+\frac{3}{2}A/\hbar)}+\frac{[P_2]_{\mathrm{av}}}{\frac{1}{2}(\Gamma+\Delta\Gamma_2)-i(\omega-A/\hbar)}\right]. \tag{20}$$

Although limited to low-temperature measurements (typically, $T<0.2$ K for ^{170}Yb in Au), this secular line shape presents the following advantages.

(i) It is simply the sum of two Lorentzian-shaped lines whose relative areas are the populations $[P_1]_{\mathrm{av}}$ and $[P_2]_{\mathrm{av}}$ of the multiplets F_1 and F_2, and whose dynamical broadenings are, respectively, the quantities $\Delta\Gamma_1$ and $\Delta\Gamma_2$ as given in (19). We plotted $\Delta\Gamma_1/C_K$ and $\Delta\Gamma_2/C_K$ as functions of T from relations (19) for $\Delta/k_B=0.11$ K; see Fig. 2. At a temperature $T=1.216\Delta/k_B=0.134$ K, the two dynamical broadenings have the same value, $\Delta\Gamma=1.2C_K/k_B$. As $C_K/2\pi$ is found to be of the order of 310 MHz K^{-1} around 0.1 K (see Sec. IV), the ratio $\hbar\Delta\Gamma/\Delta$ is less than 2×10^{-2}, justifying the use of the secular approximation in this temperature range. The asymptotic values of $\Delta\Gamma_1$ and $\Delta\Gamma_2$ (when $k_B T\gg\Delta$) are, respectively, $1.2C_K T$ and $0.8C_K T$. However, at high temperatures the secular approximation usually breaks down and the spectrum is no longer made up of two Lorentzian lines with breadths $\Delta\Gamma_1$ and $\Delta\Gamma_2$.

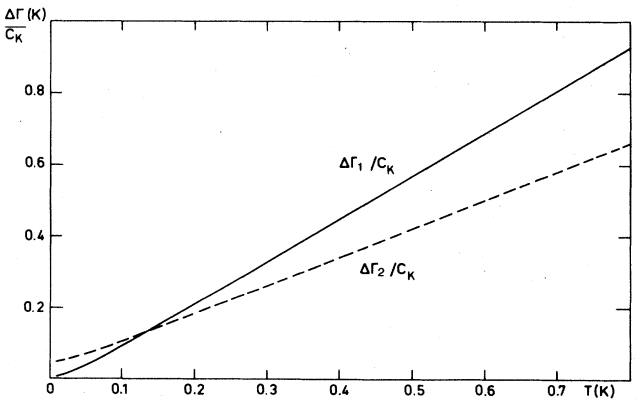

FIG. 2. Plot of the quantities $\Delta\Gamma_1/C_K$ and $\Delta\Gamma_2/C_K$ versus temperature, from relations (19). The dynamical broadenings $\Delta\Gamma_1$ and $\Delta\Gamma_2$ of lines 1 and 2 are equivalent for $T\simeq0.134$ K.

(ii) When comparing the theoretical line shapes (18) or (20) with the experimental spectrum, the natural linewidth Γ of the emission process must be replaced by the effective static linewidth $\Gamma_{\mathrm{eff}}>2\Gamma$, which includes the absorber linewidth and the instrumental line broadenings. However, compared to the general line shape (18), the secular line shape (20) offers the additional possibility of attributing different static widths Γ_1 and Γ_2 to the lines 1 and 2, and this can be useful when the inhomogeneous broadenings due to local random strains in the sample have to be taken into account.[16]

(iii) Finally, the dispersive correction[17] can be easily introduced in the Lorentzian-shaped lines of Eq. (20), allowing a better estimation of the fitted parameters.

D. C_K measurement procedure and Kondo renormalization

It is clear that the relaxation line-shape expressions (18) and (20) depend only on the temperature T and the Korringa parameter C_K, through relations (10), (15) or (16), and (19). C_K can thus be easily fitted to the experimental line shape at various temperatures. When considering the entire set of C_K fitted values, one may expect two different thermal behaviors.

(a) Observation of temperature-independent C_K fitted values would constitute evidence for Korringa behavior of the system, according to relation (4).

(b) Alternatively, a logarithmic thermal dependence of the C_K fitted values, with a negative slope, indicates Kondo behavior, as is indeed observed in the AuYb dilute alloy (cf. Sec. IV). However, the relaxation line-shape problem itself has to be reexamined in the presence of Kondo effect. In Appendix C it is shown that the line-shape ex-

pressions (18) and (20) remain valid in a good approximation if one replaces, in formulas (13), (14), and (19), the spectral densities $J(\pm\Delta)$ and $J(0)$ defined in (3), by the Kondo-modified values

$$J_K(\pm\Delta)=J(\pm\Delta)[1+a_K(T)]\ , \tag{21a}$$

$$J_K(0)=J(0)[1+b_K(T)]\ , \tag{21b}$$

where $a_K(T)$ and $b_K(T)$ are, respectively, the "inelastic" and "elastic" Kondo corrections which are defined by expressions (C6) and (C5) in Appendix C.

In its explicit form, the "elastic" Kondo correction is equal to

$$b_K(T)=4\alpha J_{sf}n(E_F)\ln|k_BT/D|\ ,$$

whence

$$J_K(0)=J(0)[1+4\alpha J_{sf}n(E_F)\ln|k_BT/D|]\ .$$

As to the "inelastic" Kondo correction $a_K(T)$, which involves the energy transfer Δ between the two hyperfine levels, it is equal to $b_K(T)$ at high temperature ($k_BT\gg\Delta$), whereas at low temperature ($k_BT\ll\Delta$) it saturates toward[11]

$$a_K(T\to 0)=4\alpha J_{sf}n(E_F)\ln|\Delta/D|\ .$$

However, using an analytical expression of $a_K(T)$ given in Ref. 18, we did not find any appreciable difference between numerical values of $1+a_K(T)$ and $1+b_K(T)$ in the temperature range of our experiments ($T\geq 0.09$ K). In these conditions the "elastic" Kondo corrective factor $1+b_K(T)$ can be used for the various spectral densities and introduced directly as a renormalization of the parameter

$$C_K=\frac{4\pi k_B}{\hbar}[\alpha J_{sf}n(E_F)]^2\ , \tag{4}$$

which has to be replaced by

$$C_{\text{Kondo}}=C_K[1+b_K(T)]$$
$$=C_K[1+4\alpha J_{sf}n(E_F)\ln|k_BT/D|]\ . \tag{22}$$

In conclusion, the fitting procedure of the spectra is the same in the Korringa and in the Kondo situations, but in the latter the fitted values of the parameter C_K are to be interpreted as C_{Kondo} values by means of relation (22) instead of (4).

III. EXPERIMENTAL SETUP

A. Mössbauer source preparation

The $Au\,^{170}$Tm sources were prepared from $5N$-purity gold supplied by Johnson-Matthey and $3N$-purity thulium supplied by Rare Earth Products. A piece of thulium (monoisotopic ^{169}Tm) with a mass of at least 2 mg (minimum allowed for easy handling) was exposed to a suitable neutron-beam irradiation in order to obtain a ^{170}Tm source with an activity of about 100 mCi. This fragment of irradiated thulium was then melted with a suitable mass of gold in a BeO crucible by setting it inside the graphite susceptor of a high-frequency induction furnace. Melting was carried out under an argon atmosphere; the susceptor and the crucible were degassed by long-duration heating prior to fusion. A preliminary 1000-ppm Tm alloy was melted, thus serving as master batch for the preparation of more dilute alloys. A piece of this master alloy, after rolling, was melted with a 4 times heavier mass of gold in order to obtain a 200-ppm Tm alloy, using the same melting conditions as above. This low concentration was necessary in order to reduce the static broadening of the lines due to crystal-field distortions.[2] The activity of the as-melted alloy was about 25 mCi, which was too high for the refrigeration capacity of our dilution apparatus. Obtaining very low temperatures demands low-activity sources, which has the drawback of requiring long counting times. A compromise was obtained with ^{170}Tm sources of a few millicuries, leading to a limiting temperature of about 0.1 K and to a recording time of about one week for each spectrum. In order to optimize experimental conditions, the radioactive alloy was rolled (between two Crysocal sheets) to a thickness of 150 μm, which gave an external activity of about half of the total activity. Ribbon pieces of area 1 to 2 cm^2 were annealed in order to eliminate defects created by cold-rolling, and then used as source samples. It was observed that insufficient annealing temperatures (e.g., 500 °C) led to broadened emission spectra, probably due to trapping of Tm impurities by defects or grain boundaries. Two samples, labeled 1 and 2, were prepared and used in the present study: Sample 1 was annealed at 750 °C for 24 h in a silica tube sealed under 10^{-6} Torr vacuum; sample 2 was annealed for 3 h at 820 °C under a dynamical secondary vacuum in a BeO crucible in the induction furnace. Finally, it is to be noted that, after any operation that could lead to a superficial contamination of the alloy (partial oxidation of the rare earth during melting or annealing, inclusion of impurities during rolling), it was subjected to intense etching by aqua regia. Additionally, the ribbon homogeneity was checked by autoradiography.

B. Sample mounting and thermometry

The sample, located outside the mixing chamber of the ^{3}He-^{4}He dilution cryostat and under vacuum, was thermalized by contact with a gold-plated copper finger, upon which it was pressed by means of an aluminium clamp and two stainless-steel screws (Fig. 3). Its temperature was measured with a carbon resistor embedded in a copper holder screwed on the clamp; since superconducting aluminium is a bad heat conductor, the clamp was covered with a thin copper sheet that is relatively transparent to γ rays; this ensured thermal contact between the carbon resistor and the sample. A second carbon resistor allows measurement of the temperature of the cold copper finger. Whereas the two carbon thermometers give the same temperature in the absence of a radioactive sample, their indications are different when the sample is inserted, the temperature of the cold finger being systematically lower than that of the sample. These measurements clearly show the existence of a thermal contact resistance between the sample, self-heated by radioactivity, and the cold finger, which takes away the heat flowing towards

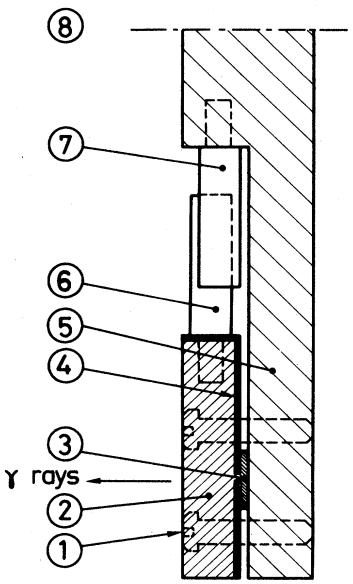

FIG. 3. Sample holder (side view). 1, stainless-steel set screw; 2, aluminium clamp, transparent to γ rays; 3, sample, clamped between parts 2 and 5; 4, thin copper sheet for thermal contact between left-hand side of sample (3) and thermometer (6); 5, cold finger of gold-plated copper linked to the dilution chamber at (8); 6, thermometer for measurements of sample temperature (3); 7, thermometer for measurements of cold-finger temperature (5); 8, towards dilution chamber.

the mixing chamber of the cryostat. Maximum temperature deviation is observed at the lowest temperatures (respectively, 0.087 K on the sample and 0.062 K on the cold finger), and the deviation becomes practically negligible above 0.16 K.

All of these results show the necessity of taking special care in measuring the temperature of radioactive samples in dilution cryostats, even for metallic samples which are good heat conductors. The precision of the sample-temperature measurement is estimated to be ± 0.004 K.

C. Spectrum recording

Mössbauer emission spectra of the $Au^{170}Tm$ source were recorded with a single-line-reference moving absorber of YbB_6 at 4.2 K, 70-at.% ^{170}Yb enriched, and containing about 33 mg of ^{170}Yb per cm^2. The minimum linewidth obtained with this absorber and a ^{170}Tm source of $TmAl_2$ was 2.7 mm s^{-1}.

The 84.3-keV γ rays were detected by an intrinsic Ge semiconductor diode. The Mössbauer drive used a symmetrical triangular velocity signal, and the symmetrical spectra recorded on the two slopes of the velocity signal were summed by folding.

IV. EXPERIMENTS AND INTERPRETATION

A. Experimental study

Preliminary data concerned partly with sample 1 were already briefly reported:[19] It was shown that the C_K fitted values decreased by about 50% between 0.1 and 4.2 K. However, measurements made in the temperature range between the two "windows" ($0.2 \lesssim T \lesssim 0.8$ K) and interpreted using the secular line shape, appeared to be unreliable. A detailed experimental study was then initiated using a new sample (no. 2), and a more general line shape [relation (18)] was used to fit the spectra of each sample.

Below, we report relaxation measurements performed between 0.108 and 4.2 K on sample 1 and between 0.087 and 4.2 K on sample 2. As the two sets of data agree with each other to within the experimental errors (cf. Figs. 5 and 6), we will not distinguish them when analyzing the results in the following.

1. Observation of hyperfine populations out of thermal equilibrium

Three emission spectra from sample 1 are shown in Fig. 4, at 0.087, 0.6, and 4.2 K, respectively. One observes on the figure a clear variation of the relative intensities of the two hyperfine components between 0.6 and 0.087 K.

As a first step, measurement of the relative intensities of the two lines was achieved by means of fitting each

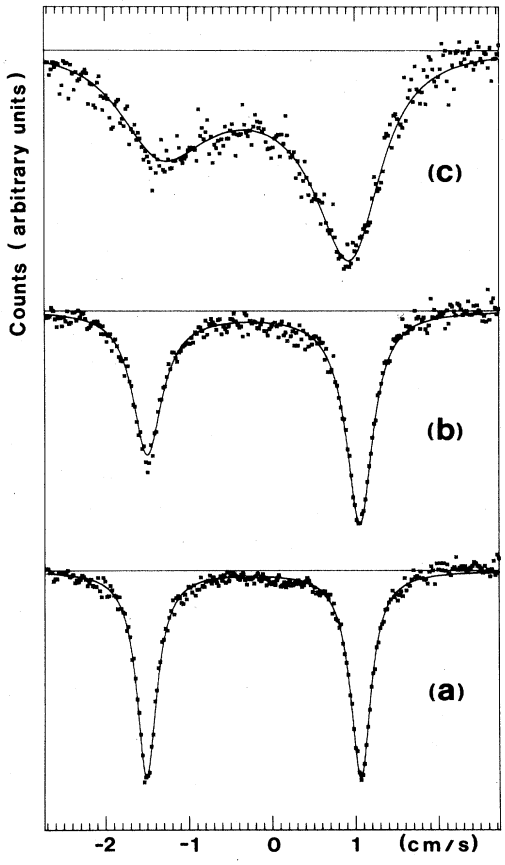

FIG. 4. Mössbauer emission spectra of $^{170}Yb^{3+}$ in gold (sample 2), at (a) 0.087 K, (b) 0.60 K, and (c) 4.2 K. Fitted curves were calculated using the general line shape expression (18), which accounts for the hyperfine populations out of thermal equilibrium.

TABLE I. Mössbauer emission spectroscopy data on $Au^{170}Yb$: Values of the relaxation parameter $C_K/2\pi$ fitted using line shapes (18) and (20), and values of the population $[P_2]_{av}$ in the F_2 hyperfine multiplet. Computed values of the Boltzmann population P_2^B in the F_2 multiplet are also given. (Note: C_K values in parentheses have been discarded in the final interpretation; see text and Fig. 6.)

T (K)	Sample no.	$C_K/2\pi$ (MHz K^{-1}) [fitted using (18)]	$C_K/2\pi$ (MHz K^{-1}) [fitted using (20)]	$[P_2]_{av}$	P_2^B
0.087	2	(353)	305	5.17	3.02
0.093	2	(347)	310	5.17	3.20
0.108	1	(354)	321	5.19	3.56
0.130	1	(358)	317	5.27	3.95
0.160	1	(332)	298	5.38	4.33
0.22	2	265	(224)	5.47	4.79
0.31	1	246	(195)	5.54	5.14
0.47	2	225		5.67	5.44
0.50	1	238		5.56	5.47
0.60	2	208		5.74	5.56
0.82	2	202			
1.43	2	200			
2.65	2	187			
4.20	1	175			
4.20	2	182			

spectrum below 0.6 K to two independent Lorentzian-shaped lines, taking into account the dispersion correction with parameter $\xi=0.015$.[17] The relative area $[P_2]_{av}$ of the right-hand line, with respect to the total area of the two-line spectrum normalized to the value 10, is given in Table I and plotted in Fig. 5 as a function of temperature. This quantity does indeed represent the population $[P_2]_{av}$ in the hyperfine multiplet F_2, as defined in (9). One can note on the figure that the $[P_2]_{av}$ measured values lie between the initial value $P_2^0=6$ and the Boltzmann curve $P_2^B(T)$ given by (6): *this clearly shows that the thermalization of the hyperfine populations in the 84.3-keV state of ^{170}Yb is not completed when the Mössbauer decay occurs.* Furthermore, at the lowest temperatures of the experiments ($T\sim0.1$ K), where the dynamical line broadenings are very small, the main information about relaxation given by the emission spectra comes from the line intensities which reflect the hyperfine populations out of thermal equilibrium.

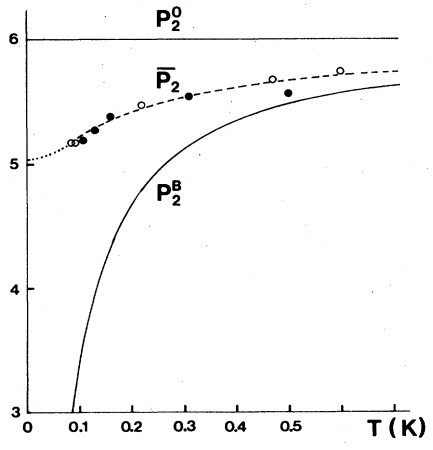

FIG. 5. Population in the upper hyperfine multiplet F_2 versus temperature: $[P_2]_{av}$, measured from the relative area of the second line (solid circles, sample 1; open circles, sample 2; dashed and dotted lines, see text). P_2^0: Initial population of F_2 just after the decay of the radioactive parent ^{170}Tm. P_2^B: Boltzmann population of F_2 computed by relation (6). Note that the total population of the 10 hyperfine levels is normalized to 10.

2. C_K measurements

All of the spectra were fitted by means of the general line shape (18): In Fig. 4 one can observe the excellent agreement between calculated curves and experimental spectra in the entire temperature range. The fitted values of the relaxation parameter C_K are given in Table I. The other parameters, i.e., the isomer shift Δ_{IS}, the hyperfine constant A, and the effective static linewidth Γ_{eff} were fitted together with C_K for each sample using the spectrum recorded at the lowest temperature. The values so obtained were then kept fixed in fitting C_K at higher temperatures.

A similar procedure was used when fitting the secular line shape (20) to the spectra; the Lorentzian-shaped lines of (20) were modified to take account of the dispersive correction.[17] Different values were allowed for the static widths Γ_1 and Γ_2 of the two lines in (20), as fitted from the lowest temperature spectra,

$\Gamma_1=3.30$ mm/s and $\Gamma_2=3.41$ mm/s for sample 1 ,

$\Gamma_1=3.35$ mm/s and $\Gamma_2=3.52$ mm/s for sample 2 .

Static line broadenings (beyond the instrumental linewidth value of $G_0=2.7$ mm/s) are due to local distortions of the cubic crystal field, originating from defects or random strains in the samples. However, in contrast with the $^{170}Yb^{3+}$ emission spectra in palladium,[16] the Γ_1 and Γ_2 values are not very different, justifying the use of the

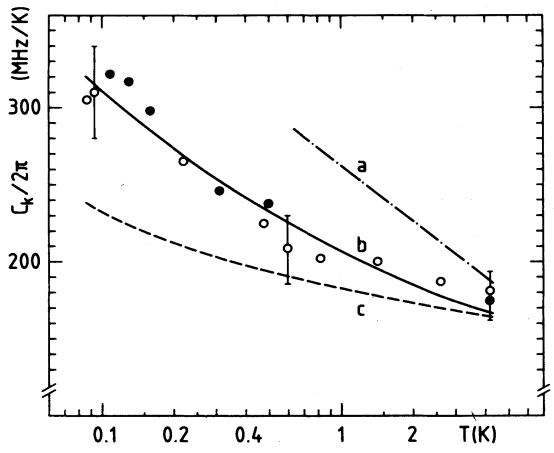

FIG. 6. Relaxation measurements in *Au*Yb. *Experimental values:* $C_K/2\pi$ values versus $\ln T$, fitted to the ^{170}Yb emission Mössbauer spectra, using line shapes (18) or (20) (see text). Solid circles, sample 1; open circles, sample 2. C_K has the physical meaning of $1/(T_1T)$ for $k_BT \gg \Delta$ and of $1/(T_{1hf}T)$ for $k_BT \sim \Delta$. The thermal variation of the C_K fitted values reveals a Kondo behavior. *Curves:* *a*, linear variation (22) of $C_{Kondo}/2\pi$ versus $\ln T$, fitted to previous "high-temperature" Mössbauer data [Ref. 1(c)]. *b*, Abrikosov-type variation (23) of $C_{Kondo}/2\pi$ fitted to the present Mössbauer data. *c*, EPR data, mean variation of $C_K/2\pi$ derived from EPR measurements [Ref. 9(b)], using relations (24) and (25).

unique linewidth parameter Γ_{eff} in the frame of the general line shape (18).

Comparing fits made using (18) and (20) calls for the following comments.

(i) At the lowest temperatures ($T \leq 0.16$ K) both types of fits give comparable values for the mean-square error $\langle \chi^2 \rangle$, but the C_K fitted values differ by about 10% (see Table I). For the reasons given in Sec. II C, we think that the more reliable values at such low temperatures are those fitted by means of the secular line shape (20).

(ii) Above 0.3 K, the $\langle \chi^2 \rangle$ values are markedly smaller when fitting the spectra by means of the general line shape (18): This shows that the secular approximation has to be discarded when the relaxation rate $1/T_1 = C_KT$ becomes comparable to about $0.04\Delta/\hbar$.

As a matter of fact, in the following we will use the C_K values fitted by means of (20) for $T \leq 0.16$ K and those fitted by means of (18) for all higher temperatures ($0.22 \leq T \leq 4.2$ K). The entire set of data is represented in Fig. 6 as a function of $\ln T$. Differences between C_K measurements from sample 1 (solid circles) and sample 2 (open circles) are not significant to within experimental errors. The interpretation of the data is given below (Sec. IV B).

3. *Other measured parameters*

The values of the isomer shift Δ_{IS} and the hyperfine constant A, fitted using the secular line shape (20) with a dispersive correction, are

$$\Delta_{IS}(\text{reference source, } TmAl_2) = (+0.164 \pm 0.040) \text{ mm/s},$$

$$A = (13.20 \pm 0.07) \text{ mm/s, or } (897 \pm 5) \text{ MHz}.$$

The isomer-shift (IS) value agrees with a previous determination[20] and can be considered as a typical value for $^{170}Yb^{3+}$ in a metallic host.

The hyperfine-constant value is very close to the values measured for the Γ_7 doublet of $^{170}Yb^{3+}$ (84.3 keV) in various insulating compounds: (896±5) MHz in CaF_2 (direct Mössbauer measurement[21]), (894±6) MHz in ThO_2, and (890±6) MHz in CeO_2 [electron nuclear double-resonance (ENDOR) measurements on $^{171}Yb^{3+}$ (Ref. 22) scaled to ^{170}Yb]. The discussion of the contribution of conduction electrons to the hyperfine constant in dilute alloys will be postponed until the end of Sec. V.

B. Interpretation of the relaxation measurements

Figure 6 shows that the C_K experimental values decrease by about 45% between 0.09 and 4.2 K, which confirms the Kondo behavior previously observed above 0.6 K.[1(b),1(c)] However, the previous measurements of $C_K = 1/(T_1T)$ using the "high-temperature" relaxation line shape (represented by the dash-dotted straight line labeled *a* in Fig. 6) were overestimated by about 25% around 1 K because of a rough determination of the static effective linewidth in these experiments.

Fitting of the C_K experimental variation by means of expression (22) of C_{Kondo}, that is, using a linear variation versus $\ln T$, gives the following values:

$$J_{sf}n(E_F) \simeq -0.078,$$

i.e., $J_{sf} \simeq -0.49$ eV using $n(E_F) \simeq 0.16$ eV^{-1} atom^{-1},[33] and

$$D \simeq 0.128 \text{ K}.$$

The value of $|J_{sf}n(E_F)|$ is slightly lower than the previous determination (-0.088 [Refs. 1(b) and 1(c)]).

However, in Fig. 6 it appears that the experimental variation of C_K versus $\ln T$ between 0.09 and 4.2 K is not exactly linear. A better fit is obtained if one uses an Abrikosov-type law[23],

$$C_{Kondo} = 2\pi B/[\ln(T/T_K)]^2, \tag{23}$$

instead of the linear variation (22) of C_{Kondo} versus $\ln T$.

The solid curve labeled *b* in Fig. 6 was fitted by means of (23), with the following parameter values:

$$B = 3.27 \times 10^4 \text{ MHz/K}, \quad T_K = 3.6 \times 10^{-6} \text{ K}.$$

C. Comparison with the EPR data

We first recall that the usual "linewidth" ΔH observed in EPR experiments, which actually is the half width at half maximum of the Lorentzian-shaped absorptive part of the dynamical transverse susceptibility $\chi_\perp(\omega)$, is written as

$$\Delta H = a(c,\omega) + \frac{\hbar}{g\mu_B}\frac{1}{T_2}, \tag{24}$$

where $a(c,\omega)$ is a residual "static" width depending on the impurity concentration c and on the resonance frequency ω, and where the second term is a dynamical broadening involving the transverse relaxation rate,

$$\frac{1}{T_2}=C_K T\left[\frac{1}{2}+\frac{\omega}{4k_B T}\coth\left[\frac{\omega}{2k_B T}\right]\right]. \tag{25}$$

In the latter expression, C_K is the Korringa constant defined in relation (4).

In the high-temperature range ($k_B T \gg \omega$), relation (25) becomes

$$1/T_2=C_K T\ , \tag{26}$$

which is equivalent to the high-temperature expression used in Mössbauer spectroscopy for $k_B T \gg \Delta$,

$$1/T_1=C_K T\ ,$$

which is relation (17). The two techniques thus measure identical quantities, $1/T_1=1/T_2$, in the high-temperature region, in the case of cubic symmetry.

At low temperature, effects due to the finite Zeeman splitting in EPR and to the hyperfine splitting in MS hinder direct comparison of the two techniques. The best solution therefore, is, to compare the experimental values of C_K, which is the only adjustable parameter of the low-temperature Mössbauer spectra and which can be extracted from the EPR linewidth via formulas (24) and (25). In the presence of the Kondo effect, expressions (22) or (23) of C_{Kondo} can be used to account for the thermal variations of the experimental fitted values of C_K in both techniques. [Note that although a frequency dependence of the C_{Kondo} values is also expected in EPR measurements,[18] this effect may be neglected for the lowest frequencies used in recent experiments, $\omega/2\pi \lesssim 3$ GHz (Ref. 9).]

EPR experiments between 1.4 and 4.2 K were performed in 1971 by Orbach and co-workers on *Au*Yb alloys using Yb concentrations down to 500 ppm.[24] The value $b=\partial\Delta H/\partial T=(40\pm10)$ G/K, corresponding to $C_K/2\pi=(187\pm47)$ MHz/K, was obtained. This mean value is in good agreement with the present Mössbauer data in the same temperature range, but the poor accuracy and the restricted temperature range did not enable a Kondo variation to be detected in these earliest EPR experiments.

Later, Baberschke and Tsang used a lower microwave frequency ($\omega/2\pi=3.22$ GHz) and extended the measurements down to about 0.1 K.[9(a)] Both linewidth and g-shift data were interpreted by Kondo variations, respectively, in $[\ln(T_K/T)]^{-2}$ and $[\ln(T_K/T)]^{-1}$, with T_K values ranging between 10^{-5} and 10^{-6} K. Concentration effects were evidenced by comparing samples with 500, 1200, and 2400 ppm of Yb.

Improved EPR data were recently published by the same group, in the temperature range 80 mK $\leq T \leq$ 4.2 K, using Yb concentrations down to 70 ppm, microwave frequencies down to 1.1 GHz, and ^{171}Yb or ^{174}Yb isotopes.[9(b)] Unfortunately, Baberschke and Tsang's recent paper contains some errors or misinterpretations which were shortly revised in a later erratum: The EPR dynamical line broadening was erroneously interpreted in terms of $1/T_1+1/T_2$ instead of $1/T_2$ as in expression (24) above. In addition, a factor of 2 was missing in the relaxation-frequency values per kelvin indicated by crosses on Figs. 4 and 6 of Ref. 9(b), which were supposed to represent our earlier Mössbauer data. Using, in turn, the EPR data given in these two figures and relation (25) of this paper, we calculated a mean "C_K" thermal variation (Fig. 6, curve c) which accounts, in a first approximation, for the EPR measurements recorded with the three microwave frequencies of $\omega/2\pi=1.1$, 3.4, and 9.0 GHz.

One observes in Fig. 6 that the EPR measurements are in good agreement with the MS values around 4 K, but they become markedly smaller at lower temperatures, the discrepancy reaching about 25% at 0.1 K. As the overall slope of the EPR variation is smaller than that for the MS variation, the associated Kondo temperature is found to be smaller as well. T_K values on the order of 10^{-8} K are derived both from EPR g-shift and relaxation data [Ref. 9(b)] and erratum instead of $\sim 10^{-6}$ K as in the present Mössbauer data.

The comparison between EPR and MS relaxation measurements calls for the following comments. Contrary to EPR, Mössbauer measurements are recorded without any applied magnetic field which could modify the Kondo properties. Furthermore, the Mössbauer measurements are less sensitive than EPR to concentration effects because the Mössbauer sample is not doped with ytterbium, but rather with dilute thulium impurities which are nonmagnetic at low temperature. Finally, as explained in Sec. II, the Mössbauer relaxation data around 0.1 K are essentially based on hyperfine-population measurements and not on dynamical line-broadening effects; the evaluation of the "static" residual linewidth thus does not present the same critical character as in EPR measurements in the slow-relaxation region. For these various reasons we think that the low-temperature Mössbauer relaxation measurements are more reliable than the corresponding EPR data.

D. Interpretation of the hyperfine-population measurements

The line-intensity or hyperfine-population data have already been exploited, together with the line broadenings, when fitting C_K by means of the relaxation line shape formulas (18) or (20). It is interesting, however, to directly compare the $[P_2]_{\text{av}}$ population measurements of Fig. 5 with the $[P_2]_{\text{av}}$ values calculated with the help of relations (10) and (16), using, in turn, the above fitted C_{Kondo} variations (22) or (23). The dashed curve in Fig. 5 was calculated down to 0.9 K using (22) with the values of the parameters $J_{sf}n(E_F)$ and D given in Sec. IV B. This curve agrees fairly well with the experimental values of $[P_2]_{\text{av}}$, but a curve calculated using (23) instead of (22) actually gives a similar agreement, which shows that $[P_2]_{\text{av}}$, measurements are not sufficient by themselves to distinguish between the two types of C_{Kondo} variations.

For $0<T<0.09$ K, that is, for $k_B T \ll \Delta$, the exact expression (15) of $1/T_{1\text{hf}}$ should be used instead of (16) when calculating $[P_2]_{\text{av}}$, and furthermore the "inelastic"

Kondo corrective factor $1+a_K(T)$ should be used in (15) instead of the "elastic" factor $1+b_K(T)$ given by (22). For $T\to 0$, both expressions (15) and $1+a_K(T)$ saturate, and the limiting values of $1/T_{1hf}$ and $[P_2]_{av}$ are[11]

$$\left.\frac{1}{T_{1hf}}\right|_{sat}=0.4\,\frac{\Delta}{k_B}C_K\left[1+4\alpha J_{sf}n(E_F)\ln\left|\frac{\Delta}{D}\right|\right],$$

i.e.,

$$\left.\frac{1}{2\pi T_{1hf}}\right|_{sat}\simeq 13.0\ \text{MHz}\ . \tag{27}$$

$$([P_2]_{av})_{sat}=\frac{P_2^0}{1+\tau_n/(T_{1hf})_{sat}}\simeq 5.04\ .$$

The dotted curve linking the calculated value of $[P_2]_{av}$ at 0.09 K to the value $([P_2]_{av})_{sat}$ at 0 K has been drawn in Fig. 5 in an attempt to represent the saturation of the $[P_2]_{av}$ thermal variation near 0 K; however, no experimental measurement was made at such low temperatures.

(We note that, apart from the saturation of the "inelastic" relaxation rate $1/T_{1hf}$ between the two hyperfine multiplets F_1 and F_2 for $k_BT\ll\Delta$, a saturation is expected in Kondo systems of both elastic and inelastic relaxation rates for $T<T_K$. As the Kondo critical temperature T_K is found to be of the order of 10^{-6} K in the system AuYb, this latter saturation phenomenon cannot obviously be observed in this alloy, but it could be of experimental interest in other cases, such as, for example, the Mössbauer study of $^{170}Yb^{3+}$ in $LaBe_{13}$.[25])

V. DISCUSSION OF THE s-f INTERACTION AND THE KONDO BEHAVIOR

For rare-earth impurities diluted in noble metals, the existence of a $5d$ virtual nonmagnetic bound state at the impurity site now seems well established.[13,26] This virtual bound state arises from resonant scattering of the $l=2$ component of the conduction electrons by the electrostatic impurity potential, and supposedly has an energy width of a few electron volts. Atomic Coulomb interaction between the rare-earth $4f$ electrons and this virtual bound state is the dominant interaction for "normal" rare earths (Er^{3+}, Dy^{3+}, etc.) in noble metals; it explains some anisotropy properties of the resistivity in these alloys rather well,[27,28] and amounts to a few tens of milli-electron-volts.

In the case of AuYb^{3+}, the existence of the Kondo effect on Yb^{3+} demonstrates that the main contribution to the interaction between the $4f$ localized electrons and the conduction electrons is resonant exchange (or s-f hybridization),[29] which yields a $4f$ magnetic virtual bound state at the impurity site, located, in energy, not far below the Fermi level, and supposedly possessing a much narrower width (a few one-hundredths of an electron volt). Our measurements of $J_{sf}\simeq -0.49$ eV, which gives the order of magnitude of the hybridization coupling, shows that atomic Coulomb interactions (~ 0.05 eV) can be neglected in the AuYb^{3+} system.

The calculation of the thermal variation of a localized-moment relaxation rate in the presence of the Kondo effect was first performed by Kondo,[30] for a spin-only moment ($S=\frac{1}{2}$), interacting with $l=0$ conduction electrons by the effective exchange interaction $\mathcal{H}_{ex}^{iso}=-2J_{sd}\vec{s}\cdot\vec{S}$. One obtains

$$\frac{1}{T_1T}=\frac{4\pi}{\hbar}[J_{sd}n(E_F)]^2k_B\left[1+4J_{sd}n(E_F)\ln\left[\frac{k_BT}{D}\right]\right]. \tag{28}$$

However, magnetic impurities usually possess orbital degeneracy, which may be partially lifted by the crystalline electric potential. In the case of d transition impurities in metallic hosts, the strong resonant hybridization with band states is supposed to obliterate the crystal-field interaction; in these alloys, Kondo properties and, in particular, relaxation-frequency measurements, are described by an effective exchange interaction between the impurity spin $\vec{S}$ and the $l=2$ partial wave of conduction electrons, with spin $\vec{s}$:

$$\mathcal{H}_{ex}=-J_{sd}P_2(\cos\theta_{\vec{k}\vec{k}'})\vec{S}\cdot\vec{s}\ ,$$

where $P_2(\cos\theta)$ is the Legendre polynomial of second order, $\theta_{\vec{k}\vec{k}'}$ is the angle between the incident ($\vec{k}$) and final ($\vec{k}'$) conduction-electron wave vectors, and J_{sd} is the effective exchange constant. Such a form for the interaction preserves the $l=2$ symmetry of the virtual bound state[31] and yields, for the relaxation rate to third order in perturbation,

$$\frac{1}{T_1}=\frac{\pi}{\hbar}k_BT\frac{[J_{sd}n(E_F)]^2}{2l+1}\left[1+2\frac{J_{sd}n(E_F)}{2l+1}\ln\left[\frac{k_BT}{D}\right]\right]. \tag{29}$$

Using a diagrammatic method, Abrikosov[23] showed that summing the most divergent terms to all orders in $J_{sd}n(E_F)$ leads to an expression for $1/T_1$ which depends only on one parameter, T_K (when $T\gg T_K$),

$$\frac{1}{T_1}=\frac{\pi}{\hbar}k_BT\frac{2l+1}{[\ln(T/T_K)]^2}$$

$$\text{where } T_K=D\exp\left[\frac{2l+1}{J_{sd}n(E_F)}\right]. \tag{30}$$

This expression takes into account the $2l+1$ orbital degeneracy of the electronic shell, the crystalline field being neglected. Furthermore, relation (29) can be considered as the first-order development of relation (30).

Thermal variation of the relaxation rate was fitted to a law of the type of (30) in CuMn ($T_K\simeq 0.01$ K) (Ref. 8) and CuFe ($T_K\simeq 30$ K) (Refs. 5 and 6). Owing to the relatively high value of T_K in these alloys, the experimental temperature range is around $10T_K$ to $100T_K$, and deviations from a linear thermal variation of the type of (29) are considerable.

For the rare-earth Kondo ions Ce^{3+} and Yb^{3+}, resonant hybridization is weaker than for $3d$ impurities and is treated as a perturbation of the crystal-field states of the rare-earth ion in the computation of the Kondo properties.[32]

At low temperature, if one considers a doublet ground state well isolated from the excited states, one can try to phenomenologically describe the Kondo interaction by an exchangelike interaction (2) with an antiferromagnetic coupling constant,

$$\mathcal{H}_{\rm sf}^{\rm eff} = -2g[(g_J-1)/g_J]J_{sf}\vec{s}\cdot\vec{S}\ ,$$

where $\vec{S}$ is the effective spin ($S=\frac{1}{2}$) of the crystal-field doublet and g is its spectroscopic constant. This is possible for Yb^{3+} since $g(g_J-1)/g_J=\alpha$ is positive for this ion, leading, hence, to Kondo properties with a negative coupling constant J_{sf}.

This approach was used throughout this paper and yields, to leading perturbation order, the thermal variation (22) of $1/T_1T$,[10,11]

$$\frac{1}{T_1T}=\frac{4\pi}{\hbar}[\alpha J_{sf}n(E_F)]^2k_B\left[1+4\alpha J_{sf}n(E_F)\ln\left[\frac{k_BT}{D}\right]\right]. \tag{22}$$

From this expression, one can derive an Abrikosov-type law,

$$\frac{1}{T_1T}=C_{\rm Kondo}=\frac{\pi k_B}{\hbar}\frac{1}{[\ln(T/T_K)]^2} \quad \text{with } T_K=D\exp\left[\frac{1}{2\alpha J_{sf}n(E_F)}\right], \tag{31}$$

that is,

$$\frac{C_{\rm Kondo}}{2\pi}=\frac{6.54\times10^4}{[\ln(T/T_K)]^2}\ \text{MHz/K}\ .$$

One cannot, however, use the same procedure for the Ce^{3+} ion, because $g_J-1<0$ for Ce^{3+}. To circumvent this difficulty, a derivation of the Kondo coupling was made by Coqblin and Schrieffer (CS),[33] who showed that in the Kondo limit the s-f—hybridization interaction can be transformed into an effective exchange interaction,

$$\mathcal{H}_{\rm CS}=-\sum_{\substack{\vec{k},\vec{k}',\\ M,M'}} J_{MM'}c^{\dagger}_{\vec{k}M}c_{\vec{k}'M'}c^{\dagger}_{M}c_{M'}\ , \tag{32}$$

where the states $|M\rangle$ and $|M'\rangle$ are eigenstates of the rare-earth ion in the crystalline electric field, $c^{\dagger}_M$ (c_M) are the creation (annihilation) operators of a localized electron in the state $|M\rangle$, $c^{\dagger}_{\vec{k}M}$ ($c_{\vec{k}M}$) are the creation (annihilation) operators of a conduction electron with wave vector $\vec{k}$ and total moment component $J_z=M$, and $J_{MM'}$ is a negative parameter depending on the energies of the ionic levels $|M\rangle$ and $|M'\rangle$ and on the hybridization coupling. In the case of Yb^{3+} (for which $J=\frac{7}{2}$), this Hamiltonian describes a j-J coupling between the local moment in the crystal field and the $j=\frac{7}{2}$ component of the itinerant-electron wave function. In terms of the resonant scattering mechanism, one can say that the $4f$ magnetic virtual bound state at the Yb^{3+} site is built up by the mixing of the crystal-field eigenstates with the eightfold-degenerate spherical component with $j=\frac{7}{2}$ of the Bloch extended states.

For an isolated doublet ground state, the CS interaction (32) yields a thermal variation of $C_{\rm Kondo}$,[3]

$$\frac{1}{T_1T}=C_{\rm Kondo}=\frac{\pi k_B}{\hbar}[J_0n(E_F)]^2\left[1+4J_0n(E_F)\ln\left[\frac{k_BT}{D}\right]\right]. \tag{33}$$

In this expression, J_0 is the negative parameter, $J_0=-|V_{kf}|^2/E_0$, where E_0 is the energy distance between the $4f$ virtual bound state and the Fermi level, and V_{kf} is a mean matrix element of the resonant mixing interaction. This variation of $C_{\rm Kondo}$ slightly differs from relation (22) mentioned above.

The Abrikosov-type law derived from expression (33) is

$$C_{\rm Kondo}=\frac{\pi k_B}{4\hbar}\frac{1}{[\ln(T/T_K)]^2} \quad \text{with } T_K=D\exp\left[\frac{1}{2J_0n(E_F)}\right]. \tag{34}$$

Expression (34) differs by a factor of 4 from expression (31): This results from the fact that the isotropic s-f exchange (2) assumes that the conduction electrons are plane waves with no orbital momentum and spin $s=\frac{1}{2}$, whereas in the CS Hamiltonian (32) we assume that they are represented by $2j+1$ partial waves, with $j=\frac{7}{2}$. The ratio 4 between the quantities $C_{\rm Kondo}=1/T_1T$ calculated with (2) or (32) simply reflects the ratio of the degeneracies $2/(2J+1)$ of the conduction states considered in the calculation of the relaxation rate.

The experimental value of the B coefficient in expression (23),

$$C_{\rm Kondo}=2\pi B/[\ln(T/T_K)]^2\ ,$$

is 3.27×10^4 MHz/K, i.e., halfway between the values calculated with (2) and (32), respectively [expressions (31) and (34)]. We have no interpretation for this result at the present moment. The authors of Ref. 9(a), in their derivation of the Abrikosov-type law, obtain a multiplicative factor α^2d, where d denotes a degeneracy or a number of "scattering channels," by analogy with $3d$ transition impurities [expression (30)]. However, the physical meaning of this degeneracy factor, left as an adjustable parameter in Ref. 9(a), remains unclear to us because the influence of the crystal field on the number of "scattering channels" is already taken into account by considering that the resonant scattering occurs within the Γ_7 ground state of the Yb^{3+} ion.

Nevertheless, our experimental results, as well as those obtained with the use of EPR in Ref. 9, demonstrate that the Abrikosov-type thermal variation of $C_{\rm Kondo}$ in the alloy $Au\,Yb^{3+}$ is more appropriate than the linear $\ln T$ law, even in a temperature range of the order of $(10^5-10^6)T_K$.

Finally, we mention that the CS Hamiltonian has been used to calculate the relaxation rate of Yb^{3+} in gold at a higher temperature,[3] when transitions toward excited crystal-field levels become important, and also in a NMR

study in the presence of a strong magnetic field which appreciably mixes the crystal-field states.[34]

We next consider the contribution of conduction electrons to the hyperfine constant A.

In dilute alloys, one expects an extra contribution ΔA to the hyperfine constant to arise from the dynamic polarization of conduction electrons via the exchange coupling.[35] A second-order perturbation calculation, with the assumption that the conduction bands have s character, shows that

$$\Delta A \sim g\frac{g_J-1}{g_J}A_{\mathrm{CE}}J_{sf}n(E_F)\ ,$$

where A_{CE} is the Fermi-contact hyperfine constant of conduction electrons at the nucleus site.

In the case of atomiclike exchange between $4f$ and conduction electrons, J_{sf} is positive, as is A_{CE}.[24]

In the presence of the Kondo effect, the covalent mixing interaction predominates, with a negative coupling constant J_{CM}. However, only the $l=3$ component of the conduction-electron wave function is coupled to the $4f$ electrons, and so there is no direct-contact interaction with the nucleus. A possible contribution to ΔA could, however, indirectly arise through core polarization of s-type inner shells, yielding

$$\Delta A \sim g\frac{g_J-1}{g_J}A^{cp}_{\mathrm{cont}}J_{\mathrm{CM}}n(E_F)\ ,$$

where A^{cp}_{cont} is the contact hyperfine interaction due to dynamical polarization of inner s shells by conduction electrons. According to Ref. 24, A^{cp}_{cont} is negative.

Thus in both cases, ΔA has the same sign as g_J-1, and should be positive for Yb^{3+}. In the Kondo alloy AuYb, the covalent mixing interaction is dominant, and thus, using the measured value of $J_{\mathrm{CM}}n(E_F)$, we obtain

$$\Delta A \sim -0.03A^{cp}_{\mathrm{cont}}\ .$$

We indeed observe a very small increment of A in AuYb with respect to the value in insulators (less than 1%). As there is no available measurement of A^{cp}_{cont} as far as we know, this might indicate that A^{cp}_{cont} is not bigger than a few hundred megahertz, which is the right order of magnitude for core-polarization effects.[36,37]

VI. CONCLUDING REMARKS

This paper shows several improvements with respect to our previous studies of the AuYb system at low temperatures.[1,2,11]

First, the use of a ^{3}He-^{4}He dilution refrigerator allowed us to extend the temperature range of the experiments down to 0.09 K, that is, below the hyperfine separation value ($\Delta/k_B=0.11$ K).

Our results clearly demonstrate the existence of hyperfine populations out of thermal equilibrium in the $Au\,^{170}$Yb emission spectra at such low temperatures. They also show that the information about electronic relaxation available from the hyperfine populations progressively overcomes the information available from dynamical line broadenings as temperature decreases. Relaxation rates down to $\frac{1}{80}(\Delta/\hbar)$ have been measured in this way.

The computation of a general relaxation line shape gave us the possibility to take all of the information present in the emission spectra in the entire temperature range into full account, including the population effects. We also computed the emission line shape within the secular approximation and compared the respective advantages of the two line shapes for fitting the low-temperature spectra.

In conclusion, this study enabled us to confirm the Kondo behavior of Yb^{3+} in gold by measuring the relaxation parameter $C_K=1/T_1T$ (or $1/T_{1\mathrm{hf}}T$ for $T\sim\Delta/k_B$) from 4.2 down to 0.09 K.

Our data are better fitted by means of an Abrikosov-type variation in $[\ln(T/T_K)]^{-2}$ than with the usual Kondo linear logarithmic dependence. The order of magnitude of the Kondo critical temperature T_K is found to be a few 10^{-6} K, that is, about 2 orders of magnitude larger than in recent EPR experiments.

ACKNOWLEDGMENTS

We thank J. F. Lericque for the construction of the ^{3}He-^{4}He dilution refrigerator and for technical assistance during the experiments.

APPENDIX A: MÖSSBAUER LINE SHAPE OF A SOURCE AT LOW TEMPERATURE IN THE ABSENCE OF THE KONDO EFFECT

1. Summary of general formulas (Refs. 10, 38, and 39)

We consider a source with an excited Mössbauer state I (electronuclear substates f) and a ground state I_g (electronuclear substates g), between which a Mössbauer transition is induced by a nuclear electromagnetic multipole T_L. It can be shown that in the Liouville formalism and within the "density-matrix" approach, the Mössbauer line shape $\mathcal{F}(\omega)$ of a powder spectrum in the presence of relaxation is given by

$$\mathcal{F}(\omega)\propto \mathrm{Re}\sum_{\substack{M,f_1,f_2,f_3,\\ g_1,g_2}}\langle f_1\,|\,T^M_L\,|\,g_1\rangle\langle g_2\,|\,(T^M_L)^\dagger\,|\,f_2\rangle\left\langle g_1,f_3\left|\frac{-1}{i\omega-\Gamma/2+(i/\hbar)\mathscr{H}^\times_0+R}\right|g_2,f_2\right\rangle\sigma^I_{f_3f_1}(1/\Gamma)\ , \qquad \text{(A1)}$$

with

$$\sigma^I_{f_3 f_1}(1/\Gamma)=\sum_{f_4,f_5}\left\langle f_3,f_1\left|\frac{-\Gamma}{-\Gamma-(i/\hbar)\mathscr{H}_0^{\times}+S}\right|f_4,f_5\right\rangle\langle f_4\,|\,\sigma^I_{\rm in}\,|\,f_5\rangle\ , \tag{A2}$$

in which we note the following. (i) $\mathscr{H}_0^{\times}$ is the atomic Liouville Hamiltonian in the absence of relaxation [we will assume that the kets $|g,f\rangle$ are the eigenstates of $\mathscr{H}_0^{\times}$, with eigenvalues E_g-E_f]. [Similarly, in the standard formalism, $|f\rangle, |g\rangle$ are the eigenstates of $\mathscr{H}_0$ with eigenvalues E_f,E_g. We recall that it is necessary to use this basis for computing relaxation effects when the white-noise approximation is not valid. It is also appropriate to the description of the density matrix of the excited state in terms of populations (see below).] (ii) R and S are (related) relaxation supermatrices.[39,40] (iii) $\Gamma=1/\tau_n$ is the linewidth of the excited Mössbauer state. (iv) $\sigma^I(1/\Gamma)$ [Eq. (A2)] is the average value of the density matrix σ of the excited Mössbauer state I in the presence of (a) feeding by the radioactive parent with rate $+\Gamma\sigma^I_{\rm in}$, (b) evolution in the presence of $\mathscr{H}_0^{\times}$, (c) relaxation S which drives σ towards the Boltzmann value σ^I_B, and (d) decay towards the Mössbauer ground state with the rate $-\Gamma\sigma$. $\sigma^I(1/\Gamma)$ is also the solution of the detailed balance equation [equivalent to Eq. (A2)],

$$\frac{d\sigma}{dt}=0=\Gamma\sigma^I_{\rm in}+\left[-\frac{i}{\hbar}\mathscr{H}_0^{\times}+S\right]\sigma-\Gamma\sigma\ . \tag{A3}$$

Owing to the properties of spontaneous emission, when the parent is at thermal equilibrium, the initial density matrix $\sigma^I_{\rm in}$ is diagonal with respect to the eigenstates $|f\rangle$ of $\mathscr{H}_0$: $f_4=f_5$.

If σ remains diagonal during its evolution, then $f_3=f_1$ in Eq. (A2); one may speak in terms of average *populations* $p_f(1/\Gamma)=\sigma_{ff}(1/\Gamma)$ and Eq. (A3) is replaced by the rate equation

$$\frac{dp_f}{dt}=0=\Gamma p_f^{\rm in}-\sum_{f'}W_{f\to f'}p_f+\sum_{f'}W_{f'\to f}p_{f'}-\Gamma p_f\ , \tag{A4}$$

in which $\mathscr{H}_0^{\times}$ has disappeared because it commutes with the populations, and the second and third terms on the right-hand side (rhs) are associated with relaxation ($W_{f\to f'}$ and $W_{f'\to f}$ are transition probabilities). The solutions of Eq. (A4) are the $p_f(1/\Gamma)$.

In terms of these populations, the Mössbauer line shape becomes

$$\mathscr{J}(\omega)\propto{\rm Re}\sum_M\sum_{\substack{f_1,f_2\\ g_1,g_2}}\langle f_1\,|\,T_L^M\,|\,g_1\rangle\langle g_2\,|\,(T_L^M)^{\dagger}\,|\,f_2\rangle\left\langle g_1,f_1\left|\frac{-1}{i\omega-\Gamma/2+(i/\hbar)\mathscr{H}_0^{\times}+R}\right|g_2,f_2\right\rangle p_{f_1}(1/\Gamma)\ . \tag{A5}$$

2. Introduction of tensor-operator formalism

We now consider the case where $\mathscr{H}_0$ is an isotropic hyperfine structure Hamiltonian: $\mathscr{H}_0=A\vec{\mathrm{I}}\cdot\vec{\mathrm{S}}$ or $A_g\vec{\mathrm{I}}_g\cdot\vec{\mathrm{S}}$ ($\vec{\mathrm{S}}$ denotes an effective electronic spin); then $|f\rangle\equiv|F,m_F\rangle$ and $|g\rangle\equiv|G,m_G\rangle$, with $\vec{\mathrm{F}}=\vec{\mathrm{I}}+\vec{\mathrm{S}}$ and $\vec{\mathrm{G}}=\vec{\mathrm{I}}_g+\vec{\mathrm{S}}$. If the relaxation process is also isotropic, it is interesting to use the tensor-operator formalism of Ref. 41. For this, the expression for $\mathscr{J}(\omega)$ is first transformed by expressing the nuclear multipole $\underset{\sim}{T}_L$ in terms of tensor operators ${}^{FG}\underset{\sim}{V}_L$ adapted to the coupled system [Ref. 40; Ref. 41, Eqs. (26)–(34)]

$$T_L^M=\sum_{F,G}b_L^{FG\,FG}V_L^M\ , \tag{A6}$$

in which the coefficient b_L^{FG} is related to a $6j$ coefficient:

$$b_L^{FG}=(-1)^{I+S+G+L}[(2F+1)(2G+1)]^{1/2}\begin{Bmatrix}F & G & L\\ I_g & I & S\end{Bmatrix}\ , \tag{A7}$$

and the tensor operator ${}^{FG}\underset{\sim}{V}_L$ is defined in terms of a Clebsch-Gordan coefficient,

$${}^{FG}V_L^M=\sum_{m_F,m_G}(-1)^{G+m_G}\langle F,m_F;G,m_G\,|\,L,M\rangle\,|\,F,m_F\rangle\langle G,-m_G\,|\ . \tag{A8}$$

The Mössbauer line shape then takes the form

$$\mathscr{J}(\omega)\propto\sum_{\substack{F,G,\\ F',G'\\ -L\le M\le+L}}b_L^{F'G'}b_L^{FG}\sum_{\substack{m_F,m'_{F'}\\ m_G,m'_{G'}}}p^F_{m_F}(1/\Gamma)\langle F,m_F\,|\,{}^{FG}V_L^M\,|\,G,m_G\rangle\langle G',m'_{G'}\,|\,({}^{F'G'}V_L^M)^{\dagger}\,|\,F',m'_{F'}\rangle$$
$$\times\left\langle G,m_G;F,m_F\left|\frac{-1}{i\omega-\Gamma/2+(i/\hbar)\mathscr{H}_0^{\times}+R}\right|G',m'_{G'};F',m'_{F'}\right\rangle\ . \tag{A9}$$

We now assume that the average populations $p^F_{m_F}(1/\Gamma)$ of the substates $|m_F\rangle$ of a hyperfine state F are all equal:

$$p^F_{m_F}(1/\Gamma)=\frac{1}{2F+1}P_F(1/\Gamma)\ . \tag{A10}$$

It becomes possible to take $P_F(1/\Gamma)$ out of the summation over m_F, $m'_{F'}$, m_G, and $m'_{G'}$. Then, for isotropic relaxation, the summation can be performed with the result

$$\mathcal{J}(\omega)\propto \mathrm{Re}\sum_{\substack{F,G,\\F',G',\\M}}\frac{P_F(1/\Gamma)}{2F+1}b_L^{FG}b_L^{F'G'}\left\langle L,M,G,F\left|\frac{-1}{i\omega-\Gamma/2+(i/\hbar)\mathcal{H}_0^{\times}+R}\right|L,M,G',F'\right\rangle\ . \tag{A11}$$

The kets $|L,M,G,F\rangle$, in which L is the multipolarity of the Mössbauer transition, are parts of a larger set of kets $|L',M',G,F\rangle$, with $|F-G|\le L'\le F+G$ for each pair F,G. With respect to this basis and when both the hyperfine Hamiltonian $\mathcal{H}_0^{\times}$ and the relaxation process are isotropic, the matrix elements of $i\omega-\Gamma/2+(i/\hbar)\mathcal{H}_0^{\times}+R$ have the form [Ref. 41, Eqs. (38)—(40); Ref. 42, Eq. (1)]

$$\left\langle L',M',G',F'\left|\left[i\omega-\frac{\Gamma}{2}+\frac{i}{\hbar}\mathcal{H}_0^{\times}+R\right]\right|L'',M'',G'',F''\right\rangle\equiv\underset{I,I_g,S}{\mathrm{Trace}}\left[({}^{G'F'}V^{M'}_{L'})^{\dagger}\left[i\omega-\frac{\Gamma}{2}+\frac{i}{\hbar}\mathcal{H}_0^{\times}+R\right]^{G''F''}V^{M''}_{L''}\right]$$

$$=\delta_{L'L''}\delta_{M'M''}\delta_{F'F''}\delta_{G'G''}\left[i\omega-\frac{\Gamma}{2}+i\omega_{G'F'}\right]+\delta_{L'L''}\delta_{M'M''}\langle L',G',F'\,|\,R\,|\,L'',G'',F''\rangle\ , \tag{A12}$$

in which, because of the projection operator which enters ${}^{G'F'}V^{M'}_{L'}$, the trace is in fact equivalent to a summation over $m'_{F'}$, $m''_{F''}$, $m'_{G'}$, and $m''_{G''}$. We observe that the large matrix factorizes into submatrices corresponding to given L' and M', and that for fixed L', the submatrices associated with different M' do not depend on M'. To obtain the Mössbauer line shape, we only need to invert the submatrix corresponding to the multipolarity L of the Mössbauer transition and to $M=0$.

In this paper we are interested in relaxation by the conduction electrons. Up to a certain stage of the calculation, this relaxation is equivalent to the more general problem of relaxation by a fluctuating isotropic quantum field. This last model will be used from Eqs. (A13) to (A25) and the specialization of the formulas to conduction electrons will be deferred until Eq. (A26).

We then consider a relaxation Hamiltonian

$$\mathcal{H}_1=-g\mu_B\vec{\mathrm{H}}(t)\cdot\vec{\mathrm{S}}\ , \tag{A13}$$

in which $\vec{\mathrm{H}}$ is a fluctuating isotropic quantum field. At high temperature and up to second order in $\mathcal{H}_1$, the relaxation coefficient $\langle L,G,F\,|\,R\,|\,L,G',F'\rangle$ associated with $\mathcal{H}_1$ is related to the spectral density $I(\omega)$ of the field $\vec{\mathrm{H}}$ by the complicated Eq. (1) of Ref. 42. At low temperatures (quantum field) two different spectral densities exist,

$$I'(\omega)=\frac{g^2\mu_B^2}{\hbar^2}\int_0^{\infty}d\tau e^{i\omega\tau}\underset{\text{lattice}}{\mathrm{Trace}}[\rho_B H^z(0)H^z(-\tau)]\ ,$$

$$I''(\omega)=\frac{g^2\mu_B^2}{\hbar^2}\int_0^{\infty}d\tau e^{i\omega\tau}\underset{\text{lattice}}{\mathrm{Trace}}[\rho_B H^z(-\tau)H^z(0)] \tag{A14}$$

(where ρ_B is the density matrix of the lattice), and in the expression of Ref. 42 for $\langle L,G,F\,|\,R\,|\,L,G',F'\rangle$, the four spectral densities I have to be replaced, respectively, by I'', I', I', and I'' (Ref. 42, note added in proof). Here we will only be concerned with a particular case of these results [see Eq. (A15) below].

3. Application to $Au^{170}Yb$

From now on we will restrict ourselves to the case of $Au^{170}Yb$, where $I=2$, $I_g=0$, $S=\frac{1}{2}$, and $L=I=2$.

In state I, $\mathcal{H}_0=A\vec{\mathrm{I}}\cdot\vec{\mathrm{S}}$ has two hyperfine eigenstates with $F=\frac{5}{2}$ and $\frac{3}{2}$ separated by $\Delta=5A/2\hbar$, and in state I_g there is a single hyperfine state with $G=S=\frac{1}{2}$. The spectrum is obtained by inversion of the submatrix $L=2,M=0$ of Eq. (A12), which is 2×2 (two pairs F,G).

We are interested in relaxation by a fluctuating quantum field. When $I_g=0$ and $L=I$, the expression for $\langle L,G,F\,|\,R\,|\,L,G,F'\rangle$ is [Ref. 42, Eq. (3) and note added in proof],

$$\langle L,G,F\,|\,R\,|\,L,G,F'\rangle=-S(S+1)\left[\delta_{FF'}\left[I''(0)+\sum_{F''}(2S+1)(2F''+1)\begin{Bmatrix}F'' & F & 1\\ S & S & I\end{Bmatrix}^2 I'(\omega_{FF''})\right]\right.$$

$$\left.+(-1)^{F+F'+2S+1}(2S+1)[(2F+1)(2F'+1)]^{1/2}\begin{Bmatrix}F' & F & 1\\ S & S & I\end{Bmatrix}^2[I'(\omega_{FF'})+I''(0)]\right]\ . \tag{A15}$$

Let us neglect the imaginary part of R. It can be shown that $\mathrm{Re}I''(-\omega)=\mathrm{Re}I'(\omega)$ and $\mathrm{Re}I'(\omega)=\exp(\hbar\omega/k_BT)\,\mathrm{Re}I'(-\omega)$ ["equilibration relation," Ref. 43, Eq. (4.67)]. We then define

$$J(0)=2\,\mathrm{Re}I'(0)\,,\quad J(\Delta)=2\,\mathrm{Re}I'(\Delta)\,,\quad J(-\Delta)=2\,\mathrm{Re}I'(-\Delta)\,, \tag{A16}$$

and

$$\Delta\Gamma_1=\tfrac{3}{5}[J(0)+J(-\Delta)],\quad \Delta\Gamma_2=\tfrac{2}{5}[J(0)+J(+\Delta)]\,. \tag{A17}$$

With the help of Eqs. (A12) and (A15), the submatrix $L=2,M=0$ of $i\omega-\Gamma/2+(i/\hbar)\mathscr{H}_0^{\times}+R$ is found to be equal to

$$\begin{matrix} G=\frac{1}{2},\ F=\frac{3}{2} \\ G=\frac{1}{2},\ F=\frac{5}{2} \end{matrix}\begin{bmatrix} i\omega-\dfrac{\Gamma}{2}+i\dfrac{3A}{2\hbar}-\dfrac{\Delta\Gamma_1}{2} & -\dfrac{\sqrt{6}}{3}\dfrac{\Delta\Gamma_1}{2} \\ -\dfrac{\sqrt{6}}{2}\dfrac{\Delta\Gamma_2}{2} & i\omega-\dfrac{\Gamma}{2}-\dfrac{iA}{\hbar}-\dfrac{\Delta\Gamma_2}{2} \end{bmatrix}, \tag{A18}$$

whence, using Eq. (A11), the Mössbauer line shape, valid for any isotropic fluctuating quantum field ($p=\Gamma/2-i\omega$),

$$\mathscr{J}(\omega)\propto \mathrm{Re}\left[\frac{P_{3/2}(1/\Gamma)[p+iA/\hbar+(\Delta\Gamma_1+\Delta\Gamma_2)/2]+P_{5/2}(1/\Gamma)[p-i(3A/2\hbar)+(\Delta\Gamma_1+\Delta\Gamma_2)/2]}{p^2-(iA/2\hbar)p+[(\Delta\Gamma_1+\Delta\Gamma_2)/2]p+3A^2/2\hbar^2-(iA/\hbar)(\frac{3}{4}\Delta\Gamma_2-\frac{1}{2}\Delta\Gamma_1)}\right]. \tag{A19}$$

Note that $P_{3/2}(1/\Gamma)$ and $P_{5/2}(1/\Gamma)$ are, respectively, $[P_1]_{\mathrm{av}}$ and $[P_2]_{\mathrm{av}}$ of the main text. The Mössbauer line shape can also be expressed in terms of the parameters

$$W=\tfrac{1}{2}J(0),\quad U=\tfrac{2}{5}J(\Delta),\quad V=\tfrac{3}{5}J(-\Delta)\,, \tag{A20}$$

which were introduced in our previous work [Ref. 2, Eq. (82); Ref. 11, Eqs. (28)—(30)] in connection with the high-temperature line shape (W) and the relaxation of the hyperfine populations (U,V). As a function of U, V, and W the line shape becomes

$$\mathscr{J}(\omega)\propto \mathrm{Re}\left[\frac{P_{3/2}(1/\Gamma)[p+iA/\hbar+W+(U+V)/2]+P_{5/2}(1/\Gamma)[p-i3A/2\hbar+W+(U+V)/2]}{p^2-(iA/2\hbar)p+[W+\frac{1}{2}(U+V)]p+3A^2/2\hbar^2-i(3A/2\hbar)(\frac{1}{2}U-\frac{1}{3}V)}\right]. \tag{A21}$$

In terms of these same parameters, the average hyperfine populations $P_{5/2}(1/\Gamma)$ and $P_{3/2}(1/\Gamma)$ of the excited Mössbauer state, which enter Eqs. (A19) and (A21), are solutions of [Ref. 11, Eq. (28)]

$$\frac{dP_{5/2}}{dt}=0=\Gamma P^0_{5/2}-UP_{5/2}+VP_{3/2}-\Gamma P_{5/2},\quad \frac{dP_{3/2}}{dt}=0=\Gamma P^0_{3/2}+UP_{5/2}-VP_{3/2}-\Gamma P_{3/2}\,, \tag{A22}$$

in which $\Gamma P^0_{5/2}$ and $\Gamma P^0_{3/2}$ are the feeding rates of the two hyperfine states by the parent, the terms in U and V are associated with relaxation between $F=\frac{3}{2}$ and $\frac{5}{2}$, and $-\Gamma P_{5/2}$ and $-\Gamma P_{3/2}$ correspond to radiative decay of I towards I_g. Only the parameters U and V appear in these equations, because relaxation processes between $F=\frac{3}{2}$ and $\frac{5}{2}$ always involve an energy transfer $\pm\Delta$ between the Mössbauer atom and the thermal bath.

Equations (A19) and (A21) have been established without the white-noise approximation. They are then valid, provided that the relaxation effects are small compared to the hyperfine interval Δ.[39,41] For Au^{170}Yb, in which $\Delta/k_B=0.11$ K, relaxation effects happen to fulfill the smallness condition below, say, 0.6 K. If they become sufficiently small for the secular approximation to apply, then we may neglect the off-diagonal elements in the matrix [Eq. (A18)], and the Mössbauer line shape (A21) reduces to the sum of two Lorentzian-shaped lines:

$$\mathscr{J}(\omega)\propto \mathrm{Re}\left[\frac{P_{3/2}(1/\Gamma)}{\frac{1}{2}(\Gamma+\Delta\Gamma_1)-i\omega-i(3A/2\hbar)}+\frac{P_{5/2}(1/\Gamma)}{\frac{1}{2}(\Gamma+\Delta\Gamma_2)-i\omega+iA/\hbar}\right], \tag{A23}$$

in which

$$\frac{\Delta\Gamma_1}{2}=\tfrac{3}{5}W+\tfrac{1}{2}V,\quad \frac{\Delta\Gamma_2}{2}=\tfrac{2}{5}W+\tfrac{1}{2}U\,. \tag{A24}$$

In contrast, at high temperature ($T>0.6$ K) the relaxation effects are no longer small, but the WNA applies since $k_BT\gg\Delta$, and Eqs. (A19) and (A21) remain valid, with $J(0)=J(\Delta)=J(-\Delta)$. In addition, the density matrix of the excited Mössbauer state is now proportional to the unit matrix, and $P_{3/2}(1/\Gamma)=4$ and $P_{5/2}(1/\Gamma)=6$. Equations (A19) and (A21) are then replaced by [Ref. 40, Eq. (34); Ref. 41, Eq. (36)].

$$\mathscr{J}(\omega)\propto 10\,\mathrm{Re}\left[\frac{p-iA/2\hbar+1/T_{1s}}{p^2+p(1/T_{1s}-iA/2\hbar)+3A^2/2\hbar^2}\right], \tag{A25}$$

with $1/T_{1s}=J(0)$.

In the case where relaxation is due to the conduction electrons,

$$\mathscr{H}_1=-2J_{sf}\alpha\vec{\mathbf{S}}\cdot\vec{\mathbf{s}}\,, \tag{A26}$$

the relaxation coefficients are given in terms of the Korringa constant

$$C_K=(4\pi/\hbar)[\alpha J_{sf} n(E_F)]^2 k_B$$

by[11]

$$J(0)=C_K T\ ,$$
$$J(\Delta)=C_K \frac{\Delta}{k_B}\frac{\exp(\Delta/k_B T)}{\exp(\Delta/k_B T)-1}\ , \tag{A27}$$
$$J(-\Delta)=C_K \frac{\Delta}{k_B}\frac{1}{\exp(\Delta/k_B T)-1}\ ,$$

whence $\Delta\Gamma_1$, $\Delta\Gamma_2$, U, V, and W are given by Eqs. (A16) and (A20).

All of the above results have been derived under the assumption that the density matrix σ of the excited Mössbauer state always remains diagonal. We must now check this point.

APPENDIX B: DECOUPLING PROBLEMS

We want to show that, in the presence of relaxation, the density matrix σ of the excited Mössbauer state I remains always diagonal, i.e., that the $p^F_{m_F}\equiv\sigma^{FF}_{m_F m_F}$ are decoupled from all other matrix element $\sigma^{F'F''}_{m'_{F'}m''_{F''}}$ with $F'\neq F''$ and/or $m'_{F'}\neq m''_{F''}$.

This was demonstrated in Ref. 10 for the case $m'_{F'}\neq m''_{F''}$ using symmetry considerations based on the isotropy of the fluctuating field. It remains to be demonstrated in the case $F'\neq F''$, $m'_{F'}=m''_{F''}$.

This can be achieved if one assumes that the initial density matrix has the following properties (satisfied in Au^{170}Yb):

(i) The substates $|F,m_F\rangle$ of a hyperfine state F are equally populated: $p_F^{m_F}\equiv\sigma^{FF}_{m_F m_F}=P_F/(2F+1)$ independent of m_F.

(ii) The off-diagonal elements are all zero: $\sigma^{F'F''}_{m'_{F'}m''_{F''}}=0$ if $F'\neq F''$ and/or $m'_{F'}\neq m''_{F''}$.

Then it can be shown that (a) the off-diagonal elements remain always zero, and (b) the populations $p^F_{m_f}\equiv\sigma^{FF}_{m_F m_F}$ of a given hyperfine state remain equal to a common value $P_F(t)/(2F+1)$, which depends on time; this second point was established in Ref. 11 under assumption (a).

We now check statement (a). The density matrix σ obeys the evolution equation [Eq. (A3)]

$$\frac{d\sigma}{dt}=\Gamma\sigma^I_{\rm in}+\left[-\frac{i}{\hbar}\mathscr{H}_0^{\times}+S\right]\sigma-\Gamma\sigma\ . \tag{B1}$$

What we must show is that in $(d/dt)\sigma^{F''F'''}_{nn}$ $(F''\neq F''')$, the contribution of the populations to the relaxation term $S\sigma$ is always zero if the populations p^F_M with given F are equal [case (b)]. This population contribution is written as

$$\sum_m \langle F'',n;F''',n\,|\,S\,|\,F,m;F,m\rangle\sigma^{FF}_{mm}$$
$$=\frac{P_F}{2F+1}\sum_m\langle F''n;F''',n\,|\,S\,|\,F,m;F,m\rangle\ , \tag{B2}$$

and we must show that the last summation over m is zero.

For reasons of simplicity, the demonstration will only be performed up to second order in the relaxation Hamiltonian $\mathscr{H}_1$. Indeed, the Kondo corrections introduced in Appendix C, which are of third order in $\mathscr{H}_1$, are always small compared to the hyperfine interval Δ and they cannot induce any appreciable coupling between the diagonal and off-diagonal matrix elements of σ.

We first assume a general relaxation Hamiltonian $\mathscr{H}_1=\sum_q K_q F_q$ (K_q denotes the atomic operator and F_q denotes the lattice operator). If only the lattice correlation functions $[F_{-q}(0)F_q(-t)]_{\rm av}$ and $[F_q(-t)F_{-q}(0)]_{\rm av}$ are nonzero, then according to Eq. (8) of Ref. 41, the matrix elements of the relaxation supermatrix S are given, up to second order in $\mathscr{H}_1$, by

$$\langle F'',n;F''',n\,|\,S\,|\,F,m;F,m\rangle=\tfrac{1}{2}\sum_q\Big[-\sum_{E,e}K^{-q}_{F'',n;E,e}K^{q}_{E,e;F,m}J'_{-qq}(\omega_{FE})\delta_{F,m;F''',n}$$
$$-\sum_{E,e}K^{q}_{F,m;E,e}K^{-q}_{E,e;F''',n}J''_{-qq}(\omega_{EF})\delta_{F,m;F,''n}$$
$$+K^{-q}_{F'',n;F,m}K^{q}_{F,m;F''',n}J''_{-qq}(\omega_{F'''F})+K^{q}_{F'',n;F,m}K^{-q}_{F,m;F''',n}J'_{-qq}(\omega_{FF''})\Big]\ , \tag{B3}$$

in which the spectral densities J'_{-qq}, J''_{-qq} are defined by Eqs. (6) and (7) of Ref. 41, and we have taken the hyperfine degeneracies into account when writing their arguments.

Here we are interested in the case where relaxation is due to a fluctuating isotropic quantum field:

$$\mathscr{H}_1=-g\mu_B\vec{H}\cdot\vec{S}\ . \tag{B4}$$

Then,

$$K_0=S_z,\quad K_1=S_+/\sqrt{2},\quad K_{-1}=S_-/\sqrt{2}\ ,$$
$$F_0=-g\mu_B H_z,\quad F_1=-g\mu_B\frac{H_-}{\sqrt{2}},\quad F_{-1}=-g\mu_B\frac{H_+}{\sqrt{2}}\ , \tag{B5}$$

and two spectral densities exist, independent of q,

$$J'_{00}(\omega)=J'_{-11}(\omega)=J'_{1-1}(\omega)=2I'(\omega)\ ,$$
$$J''_{00}(\omega)=J''_{-11}(\omega)=J''_{1-1}(\omega)=2I''(\omega)\ , \tag{B6}$$

in which $I'(\omega)$ and $I''(\omega)$ have been defined previously [Eq. (A14)].

Being independent of q, the spectral densities can be taken out of the summation over q. Using this fact we will now show that the summations over q and e in the first and second lines of Eq. (B3) are zero, and that when one calculates

$$\sum_m \langle F'',n;F''',n\,|\,S\,|\,F,m;F,m\rangle$$

[Eq. (B2)], the contribution of the third line, which involve summations over q and m, is also zero.

For this purpose, as in Eq. (50) of Ref. 41, we express the components of the electronic spin $K_0=S_z(\cdots)$ in terms of tensor operators ${}^{F'F}V_1^0(\cdots)$ adapted to the hyperfine states F,

$$S_z=\left[\frac{S(S+1)(2S+1)}{3}\right]^{1/2}{}^{SS}T_1^0=\left[\frac{S(S+1)(2S+1)}{3}\right]^{1/2}\sum_{FF'}C_1^{F'F}({}^{F'F}V_1^0)\ , \tag{B7}$$

with

$${}^{F'F}V_k^q=\sum_{m_F,m'_F}|F',m'_F\rangle(-1)^{F-m'_F}(2k+1)^{1/2}\begin{pmatrix}F' & k & F\\ -m'_F & q & m_F\end{pmatrix}\langle F,m_F|\ , \tag{B8}$$

$$C_k^{F'F}=(-1)^{S+I+F+k}[(2F+1)(2F'+1)]^{1/2}\begin{Bmatrix}S & F' & I\\ F & S & k\end{Bmatrix}\ , \tag{B9}$$

in which the large parentheses and large curly brackets denote, respectively, $3j$ and $6j$ coefficients. In terms of these, the summation over q and e in the first line of the relaxation supermatrix yields

$$\sum_q\sum_e K^{-q}_{F'',n;E,e}K^q_{E,e;F,n}\propto\left\langle F'',n\left|\sum_q(-1)^q C_1^{F''E}({}^{F''E}V_1^{-q})C_1^{EF}({}^{EF}V_1^q)\right|F,n\right\rangle\ . \tag{B10}$$

However, we have demonstrated [Ref. 41, Eq. (52)] that, for any set $\{F,F',F'',F'''\}$,

$$\sum_q(-1)^q({}^{FF'}V_k^{-q})({}^{F'''F''}V_k^q)=(-1)^{F'-F}\frac{2k+1}{2F+1}\delta_{FF''}\delta_{F'F'''}\ . \tag{B11}$$

The summation of interest here then becomes

$$(-1)^{F''-E}\frac{3}{2F''+1}C_1^{F''E}\,C_1^{EF}\delta_{F''F}\ . \tag{B12}$$

The first line of the relaxation supermatrix already contains a Kroneker δ function, $\delta_{FF'''}$, and we have assumed that $F''\neq F'''$. This line is therefore zero.

The same arguments apply to the second line. The summation over m of the first term in the third line contains

$$\sum_q\sum_m K^{-q}_{F'',n;F,m}K^q_{F,m;F''',n}\propto\left\langle F'',n\left|\sum_q(-1)^q C_1^{F''F}({}^{F''F}V_1^{-q})C_1^{FF'''}({}^{FF'''}V_1^q)\right|F''',n\right\rangle$$
$$=(-1)^{F-F''}\frac{3}{2F''+1}C_1^{F''F}\,C_1^{FF'''}\,\delta_{F'''F''}\ , \tag{B13}$$

which is also zero since $F'''\neq F''$—and similarly for the last term of the third line. Consequently, when the p_m^F are independent of m, the $\sigma_{nn}^{F''F'''}$ with $F''\neq F'''$ remain always zero. [This demonstration can easily be adapted to the case where the K_q are the components of a tensor operator $T_k^q(S)$ with $k>1$ (here, $k=1, T_1^q$ is a vector).]

APPENDIX C: MÖSSBAUER LINE SHAPE OF Yb^{3+} IN GOLD IN THE PRESENCE OF THE KONDO EFFECT

The coupling of $\vec{S}$ with the conduction electrons is

$$\mathscr{H}_1=-2J_{sf}\alpha\vec{S}\cdot\vec{s}\ . \tag{C1}$$

While standard relaxation coefficients are of the order J_{sf}^2, Kondo corrections are associated with terms of order J_{sf}^3 in the relaxation supermatrix.

In Ref. 10 we showed that when either the white-noise approximation or the secular approximation is valid, these third-order terms can be simply obtained by replacing, in the relaxation matrix, the first-order transition *amplitude* A_1 by the sum of the first- and second-order transition amplitudes A_1+A_2, and by extracting the contributions of the type $A_1A_1^\dagger$ and $A_1^\dagger A_1\sim J_{sf}^2$ (standard relaxation), and of the type $A_1A_2^\dagger$ and $A_2A_1^\dagger\sim J_{sf}^3$ (Kondo corrections).

With the use of this method, it can be established (Ref. 10, Sec. V B; Ref. 11, Sec. II B) that in the presence of the Kondo effect the relaxation parameters W, U, and V, [Eqs. (A20)] should be replaced, respectively, by

$$W_K = W[1+b_K(T)] , \tag{C2}$$

$$U_K = U[1+a_K(T)] , \tag{C3}$$

$$V_K = V[1+a_K(T)] , \tag{C4}$$

with, as a function of

$$g(\epsilon_k) = \frac{1}{N}\sum_{\vec{k}'} \frac{f_{k'} - \frac{1}{2}}{\epsilon_{k'} - \epsilon_k}$$

(in which ϵ_k denotes the conduction-electron energy and f_k denotes the Fermi distribution function),

$$b_K(T) = \frac{4J_{sf}\alpha \sum_{\vec{k},\vec{k}'} g(\epsilon_k)(1-f_{k'})f_k\delta(\epsilon_k - \epsilon_{k'})}{\sum_{\vec{k},\vec{k}'} (1-f_{k'})f_k\delta(\epsilon_k - \epsilon_{k'})}$$

$$= 4J_{sf}\alpha n(E_F)\ln|k_BT/D| \tag{C5}$$

(standard elastic Kondo correction), and

$$a_K(T) = \frac{4J_{sf}\alpha \sum_{\vec{k},\vec{k}'} g(\epsilon_k)(1-f_{k'})f_k\delta(\epsilon_k - \epsilon_{k'} + \Delta)}{\sum_{\vec{k},\vec{k}'} (1-f_{k'})f_k\delta(\epsilon_k - \epsilon_{k'} + \Delta)} \tag{C6}$$

(inelastic Kondo correction associated with the hyperfine energy transfer Δ).

In Ref. 11 it was indicated that at high T ($k_BT \gg \Delta$), $a_K(T) = b_K(T)$, and that when $T \to 0$, and to first order in Δ/D (assumed to be small),

$$a_K(T) \to 4J_{sf}\alpha n(E_F)\ln|\Delta/D| , \tag{C7}$$

i.e., the inelastic Kondo correction saturates when $k_BT \ll \Delta$, this being clearly related to the energy transfer Δ involved in the relaxation between the two hyperfine states.

Since the hyperfine interval $\Delta = 0.11$ K, at temperatures $T > 0.6$ K the WNA is expected to apply. On the other hand, as shown in Fig. 4, below 0.6 K relaxation broadening is small compared to the hyperfine splitting, so we tend toward the secular approximation. We may therefore hope that the Kondo corrections a_K and b_K may be used in the entire temperature range.

[1](a) F. Gonzalez-Jimenez and P. Imbert, Solid State Commun. **11**, 861 (1972); (b) **13**, 85 (1973); (c) in *Proceedings of the International Conference on Magnetism, Moscow, 1973* (Nauka, Moscow, 1974).

[2]F. Gonzalez-Jimenez, P. Imbert, and F. Hartmann-Boutron, Phys. Rev. B **9**, 95 (1974); **10**, 2134(E) (1974).

[3]F. Gonzalez-Jimenez, B. Cornut, and B. Coqblin, Phys. Rev. B **11**, 4674 (1975).

[4]A. P. Murani, Solid State Commun. **12**, 295 (1973).

[5]M. Loewenhaupt and W. Just, Phys. Lett. **53A**, 305 (1975).

[6]O. Kanert, M. Mali, K. Preusser, and M. Mehring, Solid State Commun. **21**, 1047 (1977).

[7]H. Alloul, Physica **86&88B**, 449 (1977).

[8]H. Alloul, F. Hippert, and H. Ishii, J. Phys. F **9**, 725 (1979).

[9](a) K. Baberschke and E. Tsang, Phys. Rev. Lett. **45**, 1512 (1980); (b) Y. Von Spalden, E. Tsang, K. Baberschke, and P. Schlottmann, Phys. Rev. B **28**, 24 (1983); **29**, 487(E) (1984).

[10]F. Hartmann-Boutron, Phys. Rev. B **10**, 2113 (1974).

[11]F. Gonzalez-Jimenez, F. Hartmann-Boutron, and P. Imbert, Phys. Rev. B **10**, 2122 (1974).

[12]F. Gonzalez-Jimenez, F. Hartmann-Boutron, P. Imbert, B. Cornut, and B. Coqblin, J. Phys. (Paris) Colloq. **35**, C6-421 (1974).

[13](a) G. Williams and L. L. Hirst, Phys. Rev. **185**, 407 (1969); (b) A. P. Murani, J. Phys. C Suppl. **2**, S-153 (1970).

[14]L. L. Hirst, Phys. Rev. **181**, 597 (1969).

[15]P. Bonville, C. Garcin, A. Gérard, P. Imbert, and G. Jéhanno, Phys. Rev. B **23**, 4293 (1981); **23**, 4310 (1981).

[16]P. Bonville, F. Gonzalez-Jimenez, P. Imbert, G. Jéhanno, L. C. Lopes, A. K. Bhattacharjee, and B. Coqblin, J. Phys. (Paris) **45**, 467 (1984).

[17]P. B. Russel, G. L. Latshaw, S. S. Hanna, and G. Kaindl, Nucl. Phys. A **210**, 133 (1973).

[18]A. K. Bhattacharjee and B. Coqblin, Solid State Commun. **18**, 1587 (1976).

[19]P. Bonville, F. Gonzalez-Jimenez, P. Imbert, G. Jéhanno, and J. F. Lericque, in *Proceedings of the International Conference on the Applications of the Mössbauer Effect, Jaipur (India), 1981* (Indian National Academy, New Delhi, 1982), p. 807.

[20]P. Bonville, P. Imbert, G. Jéhanno, and F. Gonzalez-Jimenez, J. Phys. Chem. Solids **39**, 1273 (1978).

[21]C. Borely, F. Gonzalez-Jimenez, P. Imbert, and F. Varret, J. Phys. Chem. Solids, **36**, 683 (1975).

[22]J. M. Baker, T. R. Reddy, and R. L. Wood, J. Phys. C **12**, 3317 (1979).

[23]A. A. Abrikosov, Physics **2**, 5 (1966).

[24](a) L. J. Tao, D. Davidov, R. Orbach, and E. P. Chock, Phys. Rev. B **4**, 5 (1971); (b) E. P. Chock, D. Davidov, R. Orbach, C. Rettori and L. J. Tao, *ibid.* **5**, 2735 (1972). The formula given in Ref. 24(b) for ΔA is slightly erroneous: One should read $g/2$ instead of $1/g_e\mu_e$.

[25]P. Bonville, P. Imbert, and G. Jéhanno, in Proceedings of the International Conference on the Applications of the Mössbauer Effect, Alma-Ata, U.S.S.R. (1983) (unpublished).

[26]R. Devine, J. Phys. F **4**, 1447 (1974).

[27]A. Fert, R. Asomoza, D. H. Sanchez, D. Spanjaard, and A.

Friedrich, Phys. Rev. B **16**, 5040 (1977).
[28]A. Fert and P. M. Lévy, Phys. Rev. B **16**, 5052 (1977).
[29]B. Coqblin, J. Phys. (Paris) Colloq. **32**, C1-599 (1971), and references therein.
[30]J. Kondo, in *Solid State Physics,* edited by F. Seitz, D. Turnbull, and H. Ehrenreich (Academic, New York, 1969), Vol. 23, p. 223.
[31]B. Caroli, J. Phys. F **5**, 1399 (1975).
[32]B. Cornut and B. Coqblin, Phys. Rev. B **5**, 4541 (1972).
[33]B. Coqblin and J. R. Schrieffer, Phys. Rev. **185**, 847 (1969).
[34]D. Follstaedt and A. Narath, Phys. Rev. B **19**, 1374 (1979).
[35]L. L. Hirst, Z. Phys. **245**, 378 (1971).
[36]Y. Berthier, R. A. B. Devine, and E. Belorizky, Phys. Rev. B **17**, 4137 (1978).
[37]J. M. Baker, W. B. J. Blake, and G. M. Copland, Proc. R. Soc. London, Ser. A **309**, 119 (1969).
[38]F. Hartmann-Boutron and D. Spanjaard, J. Phys. (Paris) **36**, 307 (1979).
[39]F. Hartmann-Boutron, Rev. Phys. Appl. **18**, 431 (1983).
[40]C. Chopin, D. Spanjaard, and F. Hartmann-Boutron, J. Phys. (Paris) Colloq. **37**, C6-73 (1976).
[41]F. Hartmann-Boutron, J. Phys. (Paris) **40**, 57 (1979).
[42]F. Hartmann-Boutron, J. Phys. (Paris) **41**, 1289 (1980).
[43]F. Hartmann-Boutron, Ann. Phys. (Paris) **9**, 285 (1975).